DEVELOPMENT AND TESTING OF A ROTATING DETONATION ENGINE RUN ON HYDROGEN AND AIR

THESIS

Jason C Shank, 2Lt, USAF

AFIT/GAE/ENY/12-M36

DEPARTMENT OF THE AIR FORCE
AIR UNIVERSITY

AIR FORCE INSTITUTE OF TECHNOLOGY

Wright-Patterson Air Force Base, Ohio

AFIT/GAE/ENY/12-M36

DEVELOPMENT AND TESTING OF A ROTATING DETONATION ENGINE RUN ON HYDROGEN AND AIR

THESIS

Presented to the Faculty

Department of Aeronautics and Astronautics

Graduate School of Engineering and Management

Air Force Institute of Technology

Air University

Air Education and Training Command

In Partial Fulfillment of the Requirements for the

Degree of Master of Science in Aeronautical Engineering

Jason C Shank, BS

2Lt, USAF

March 2012

AFIT/GAE/ENY/12-M36

DEVELOPMENT AND TESTING OF A ROTATING DETONATION ENGINE RUN ON HYDROGEN AND AIR

Jason C Shank, BS

2Lt, USAF

Approved:

_____	_____
Paul I. King (Chairman)	Date
_____	_____
Frederick R. Schauer (Member)	Date
_____	_____
Capt Jay Rutledge (Member)	Date

Abstract

Rotating detonation engines (RDEs) have the potential for greater efficiencies over conventional engines by utilizing pressure gain combustion. A new modular RDE (6 in diameter) was developed and successfully run on hydrogen and standard air. The RDE allows for variation of injection scheme and detonation channel widths. Tests provided the operational space of the new RDE as well as characterized detonation unsteadiness. It was found that a smaller equivalence ratio than previous was required to obtain continuous detonations. Also discovered was V_{CJ} was reached in the RDE, but not sustained.

Acknowledgements

First, I am thankful to Dr. King for the opportunity to work on such a project. I am also thankful to him for his numerous hours spent critiquing my data, written work, and presentation slides. His advice and guidance was priceless.

Second, I am thankful to Dr. Schauer for allowing me to work in the DERF. The DERF is a very special place, and I am extremely proud to be part of its engineering lineage.

I am also thankful to Dr. James Karnesky. His guidance in designing the engine and answering any questions I had helped immensely. He was always quick to help me synthesize ideas and give suggestions that helped me better my research.

Also, thanks to Curt Rice and Justin Gofena for their technical expertise. They would drop anything they were working on to help me or answer any questions. They prevented many headaches and most importantly, helped keep me safe working in the lab.

I would also like to thank John Hoke, Andrew Naples, Jim Suchoki, Brian Sell, and Chris Stevens for sharing their knowledge of rotating detonation engines and working in a lab environment.

Last, but certainly not least, Rachel Russo deserves a big thank you. She was willing to take the time to assist me in reducing the data I collected and answer any questions that I had. She was an invaluable resource.

Table of Contents

Page

List of Figures

Page

List of Tables

List of Symbols

Acronyms

AFRL	Air Force Research Laboratory
CFD	Computational fluid dynamics
CJ	Chapman-Jouguet
DERF	Detonation Engine Research Facility
NRL	Naval Research Laboratory
PDE	Pulsed detonation engine
RDE	Rotating detonation engine

Symbols	[SI units] {English units}
c	speed of sound [m/s] {ft/s}
C_p	constant pressure specific heat [J/(kg*K)] {BTU/(lbm*R)}
C_v	constant volume specific heat [J/(kg*K)] {BTU/(lbm*R)}
d	diameter [m] {ft}
h	specific enthalpy [J/g] {BTU/lbm}
$h_f°$	enthalpy of formation [J/mol] {BTU/mol}
h*	critical propellant height [m] {ft}
m_dot	mass flow rate [g/s] {lbm/s}
M	Mach number
n	total number of variables
N	total number of data points in a sample
P	pressure [atm] {psi}
q	heat release [J/g] {BTU/lbm}
R	universal gas constant [J/(mol*K)] {(ft^3*psi*lbm)/(mol*R)}
s	entropy [J/K] {BTU/R}
S_x	sample standard deviation
T	temperature [K] {R}
u	velocity [m/s] {ft/s}
ν	specific volume [m^3/g] {ft^3/lbm}
V	volume [m^3] {ft^3}
x	number of consecutive points above threshold
X_bar	sample mean
Y	mass fraction

Greek Symbols	[SI units] {English units}
γ	specific heat ratio
Δ	channel width [m] {ft}
η	thermal efficiency
λ	detonation cell size [mm] {in}

Greek Symbols (continued)

ρ	density [g/m^3] {lbm/ft^3}
φ	equivalence ratio

Subscripts

b	back
B	Brayton
c	chamber
D	detonation
f	fuel
H	Humphrey
i	individual
j	individual
min	minimum
ref	reference
tot	total

DEVELOPMENT AND TESTING OF A ROTATING DETONATION ENGINE RUN ON HYDROGEN AND AIR

CHAPTER 1. INTRODUCTION

Decreasing budgets and increasing fuel prices have highlighted a need to reduce the Air Force's petroleum consumption. Subsequently, the Air Force has launched a two-pronged initiative into combating their petroleum consumption. The first is an investigation into the fuel that is used. The second initiative is an investigation into creating a more efficient engine.

Existing jet engines burn fuel through a subsonic process called deflagration. Deflagration is characterized as having a subsonic flame speed as well as being approximately constant pressure. Current research has focused on burning fuel through a supersonic process called detonation. Detonation is characterized as having a supersonic flame coupled with a shock wave. The combination of high flame speed and a shock wave produces a high-pressure region immediately behind the detonation front. Thus, the combustion process is considered to be nearly constant volume.

A constant volume process leads to higher efficiencies than a constant pressure process.[1] Efficiency of a deflagration engine for an ideal Brayton cycle depends on the temperature before and after isentropic expansion. Efficiency of a detonation engine is calculated from an ideal Humphrey cycle, and depends on the temperature before and after isentropic expansion as well as before and after combustion. Figure 1 shows the temperature-entropy and pressure-volume diagrams for the Brayton and Humphrey cycles.

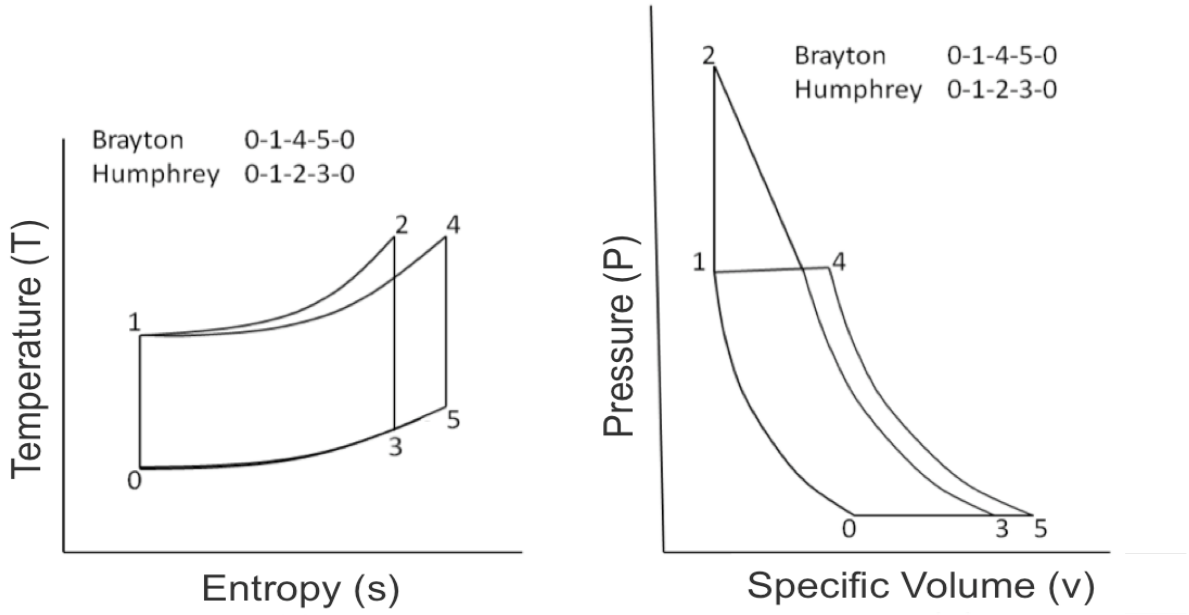

Figure 1. T-s and p-v diagrams for Brayton and Humphrey cycles[11]

The pressure spike between states 1 and 2 represents pressure gain combustion in detonation engines. The added area under the p-v curve ultimately results in increased efficiencies.

1.1 Past Research

Russian scientists performed foundational RDE experimental research in the 1960s by characterizing the structure of spinning detonation waves propagating down the length of a detonation tube.[2] They showed that a continuous detonation process could be achieved in properly sized annular detonation channels.[3] They also showed that a transverse detonation wave could be sustained with an radial injection system.[3] Other than proving the viability of RDEs, however, little research has been done since to understand the flow field within the detonation channel.

Lately, there has been a renewed focus to understand and develop RDEs due to their advantages over conventional gas turbine combustors and PDEs. Naval Research Laboratory scientists concluded that while the RDE flow field is complicated, it closely follows the thermal detonation cycle.[4] It was also concluded in a separate numerical investigation[5] that the annular detonation chamber could be connected to an axial injection system in which air and fuel mix between detonation waves. This coupling of an axial inlet system and a tangential detonation wave forms the foundation of experimental RDE research.

1.2 Current Research Objectives

The current research objectives include the development of a new RDE in which the injection and detonation channel characteristics can be changed and the mapping of an operational space based on a variation of total mass flows and equivalence ratios. Another objective includes characterizing the detonation wave as it travels around the detonation channel.

1.3 Chapter Preview

Chapter 2 contains a discussion on pulsed and continuous detonation engines. Chapter 3 details the engine development, test set-up, and data reduction techniques. Results are reported in Chapter 4. Conclusions and recommendations for future work are found in Chapter 5.

CHAPTER 2. LITERATURE REVIEW

Pressure gain combustion research was first performed in the late 1800s. Initial research focused on one-dimensional analysis of a detonation wave.[5] Early research led to the theoretical developments of the Rankine-Hugonoit curve and Zeldovich, von Neumann, and Döring's model of the structure of a detonation wave.[6] The Rankine-Hugonoit curve established two types of detonation (strong and weak) and defined the velocity at which a detonation travels (V_{CJ}). Initial experimentation focused mainly on PDEs, leaving RDE research far behind. Lately, there has been renewed vigor into RDE research due to their quasi-steady exhaust, size, and simplicity in design.

2.1 Pulsed and Rotating Detonation Engines

PDEs operate via distinct, separate phases in their combustion process.[1] Figure 2 illustrates this process.

Figure 2. PDE combustion process

A tube is initially filled at its closed end with a stoichiometric ratio of oxidizer and fuel. The mixture is then ignited. The flame travels axially towards the open end of the tube, transitioning from a subsonic deflagration to a supersonic detonation. The detonation wave eventually exits the open end of the tube. Finally, the hot products are purged from the tube, and the entire process repeated. Each phase in the process is distinct and segmented, and every detonation wave must be individually ignited.

Unlike PDEs, RDEs operate in a simultaneous and continuous manner. Figure 3 illustrates an RDE's combustion process.

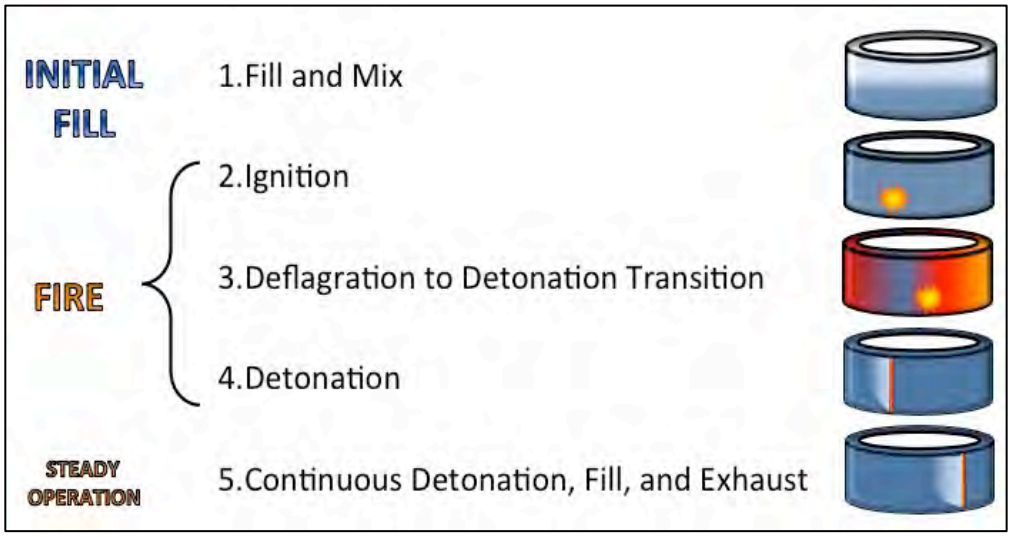

Figure 3. RDE Combustion process

An RDE must be initially filled with reactants and ignited like a PDE. Rather than initiating a deflagration that travels axially, however, a tangential and circumferential deflagration is ignited. The subsonic deflagration transitions to a supersonic detonation as it travels around the detonation channel. Eventually, a steady state is achieved in which fresh reactants fill behind the detonation front and exhaust gases expand out the

top of the RDE. Rather than a distinct, segmented process, as with a PDE, the process is simultaneous and continuous.

The continuous detonation in an RDE is an advantage. Sequential detonation PDEs are limited to a frequency of operation of approximately 100Hz. RDEs' frequency of operation, however, is in the kHz range. This high operational frequency produces a quasi-steady exhaust which is much more amenable to integration with downstream components such as a turbine.

Another advantage of an RDE is the simplicity of design. A tube-type PDE requires check valves in its closed end to control the flow of oxidizer and fuel into the tube. RDEs, however, have no moving parts. Rather, RDEs rely on manifold pressures to control the flow of oxidizer and fuel into the combustion chamber.

One final advantage of an RDE is its size. One reason is the absence of moving parts. The main reason, however, is the detonation channel. In a PDE detonation occurs axially with a length of tube solely devoted to detonation to deflagration transition (DDT). In an RDE there is no need for such a section since the detonation channel runs circumferentially and the detonation wave passes through the same space in which DDT occurs.

2.2 Experimental Rotating Detonation Engine Research

Russian scientists first characterized the nature of a spinning detonation down the length of a combustion tube.[2] The detonation traveled in a helical trajectory, proved with photographs taken of the luminosity field and density gradients.

The same Russian research also achieved a continuous detonation by pairing a radial flow with a transverse detonation wave.[2] Acetylene and oxygen flowed radially into the combustion chamber through small slits. As the detonation traveled transversely, fresh reactants filled behind the wave. One observed phenomena are two stable velocity regimes. The first velocity seen was approximately the CJ velocity. The second regime observed was approximately one-third of the CJ velocity. It was hypothesized that the detonation varied between deflagration and detonation during operation.

Russian scientists again showed significant progress in continuous detonations 50 years later.[3] Various schemes of detonation channel geometry and fuel type were tested. From the tests it was concluded that nearly all gaseous or liquid hydrocarbon fuels mixed with gaseous oxygen or air can be burnt in an annular combustion chamber in the regime of a continuous detonation. Also concluded was that a stable and continuous detonation can be achieved as long as the combustion annulus is larger than the minimum critical size of the detonation wave front. Minimum critical size is defined as the detonation cell size. Cell size depends on pressure, fuel type, and oxidizer oxygen concentration. An annular cylinder (as shown in Fig. 4) with proper width is a suitable combustion chamber for nearly all cases.

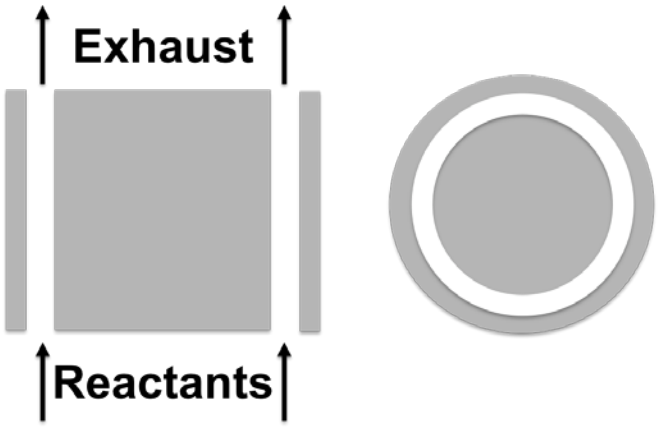

Figure 4. Side and top view of annular combustion chamber

Bykovskii et al.[3] also observed that the stability of the continuous detonation is highly dependent on the mixing of the oxidizer and fuel.

2.3 CFD Rotating Detonation Engine Research

Russian advancement in experimental understanding of continuous detonations did little to describe the flow field within the combustion chamber. Numerical investigations to fill the void in continuous detonation research have more recently been done.[7,8,9] Japanese researchers performed early RDE CFD.[7] In their simulation they used an RDE with premixed fuel and oxidizer injected axially into the detonation channel. Using a simplified chemistry model, they were able to numerically stabilize a detonation traveling at V_{CJ}. This showed that a detonation traveling at V_{CJ} could be sustained in a combustion annulus.

French and Russian researchers furthered understanding of the RDE internal flow field by using a detailed thermochemical model.[9] Again, premixed reactants (H_2 and O_2 in this case) were injected axially. Numerical results showed that the time between

passing detonation wave fronts and the injection total pressures are scaling factors for the geometry and pressure of reactive flow, respectively.

Naval Research Lab (NRL) scientists launched a computational analysis to better describe the flow field within the detonation channel.[4] In their model they used an RDE with premixed fuel and oxidizer injected in the axial direction and employed solution algorithms previously used in PDE work. They began with the 3D solution seen in Fig. 5.

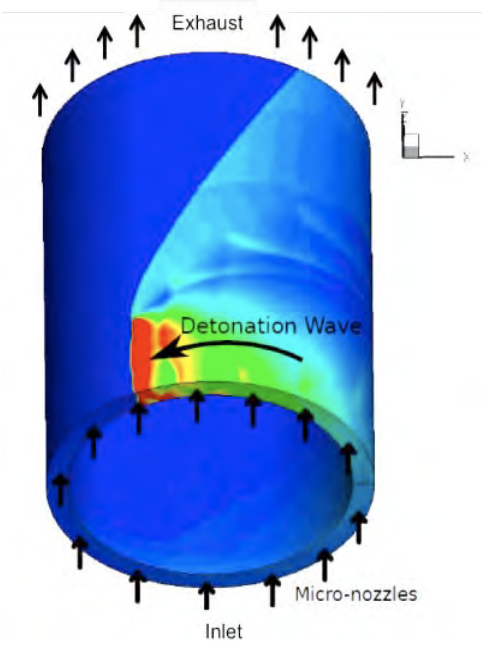

Figure 5. Schematic of 3D RDE solution[4]

The 3D solution showed little variation across the entire flow field in the radial direction, primarily due to the small radial dimension. The discovery of the small radial variation permitted the RDE to be theoretically unrolled and analyzed in two dimensions (the axial and azimuthal dimensions). Figure 6 shows the unrolled RDE. Letters mark key features in the modeled flow.

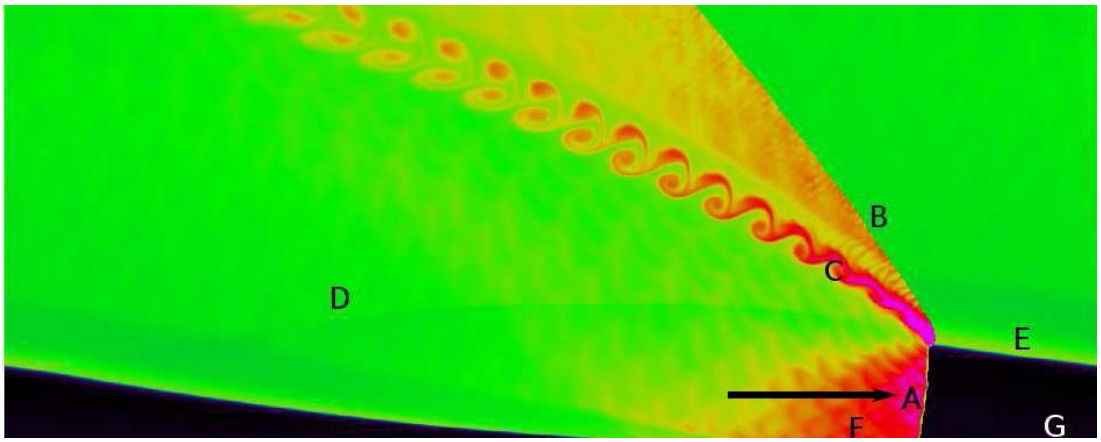

Figure 6. CFD model of unrolled RDE[4]

The key features are the (A) detonation wave, (B) oblique shock wave, (C) mixing region between the new and old detonation products, (D) secondary shock wave, (E) region of non-detonation burning that occurs at the interaction between (G) fresh propellant and hot products, and (F) the high pressure region just behind the detonation wave where reactant injection is temporarily blocked.[4]

The 2D model in Fig. 6 allowed NRL scientists to perform a parametric study on the impact of stagnation pressure, temperature, and backpressure on the mass flow, specific impulse, and detonation velocity for a constant geometry. The study showed that specific impulse depends mostly on the pressure ratio between the inlet stagnation pressure (P_o) of the reactants and back pressure (P_B) from the detonation channel. I_{sp} increases as P_o/P_B increases, however, efficiency decreases with a pressure ratio less than 10. NRL scientists also showed that mass-flow and thrust were mostly dependent on the inlet stagnation properties for a fixed geometry.[4]

NRL computationally modeled discrete injection in an RDE[8] after their continuous injection study. In the study the effect of discrete injectors on wave structure

and feedback into the mixture plenum were studied. Three different injection schemes were studied: slot micro-injectors, cylindrical micro-injectors, and a pintle injector. The 3D solution for the cylindrical micro-injectors is shown in Fig. 7.

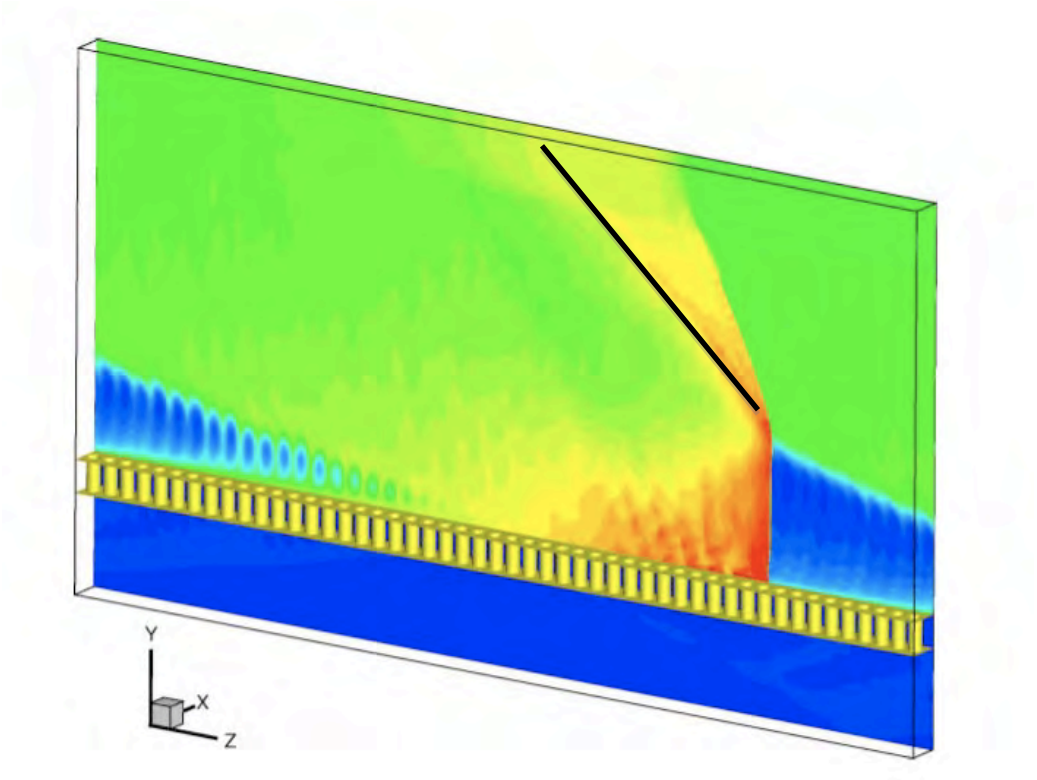

Figure 7. 3D solution for cylindrical micro-injectors in an unrolled RDE with premixing[8]

A similar wave structure as seen in Fig. 6 is present; however, there are slight differences. The first difference lies in the recovery zone immediately behind the detonation front where the discrete injection in Fig. 7 introduces discontinuities. The second difference is the absence of vortices along the secondary shock; denoted by a black line in Fig. 7 and seen in (C) of Fig. 6.

Differences in performance characteristics between the discrete micro-injectors in Fig. 7 and the ideal injectors in Fig. 6 were also noted.[8] Researchers found for all discrete injectors the detonation was stable across a smaller range of pressure ratios

(P_o/P_B) for both high and low pressures compared to ideal injectors. That being noted, micro-injector pressure losses only differed from the ideal injectors by an average of 5.9%. Also in the study, no reverse mass flow into the mixture plenum was evident; though pressure feedback was significant.

2.4 Recent Experimental Rotating Detonation Engine Research

Recent experimental research on RDEs has been on hydrogen-air systems.[3, 10, 11, 12] Much experimental work has been performed in the DERF at AFRL. Previous (to this study) work was focused on the buildup and testing of 3 in diameter RDE originally designed for ethylene and oxygen, but modified for use with air and hydrogen.

Early testing on the rig proved unsuccessful in achieving pressure gain combustion.[10, 11] Much was learned, however, and the operational regions for hydrogen-enriched air (23% O_2) and hydrogen-standard air (21% O_2) have been mapped[11] (shown in Figs. 8 and 9).

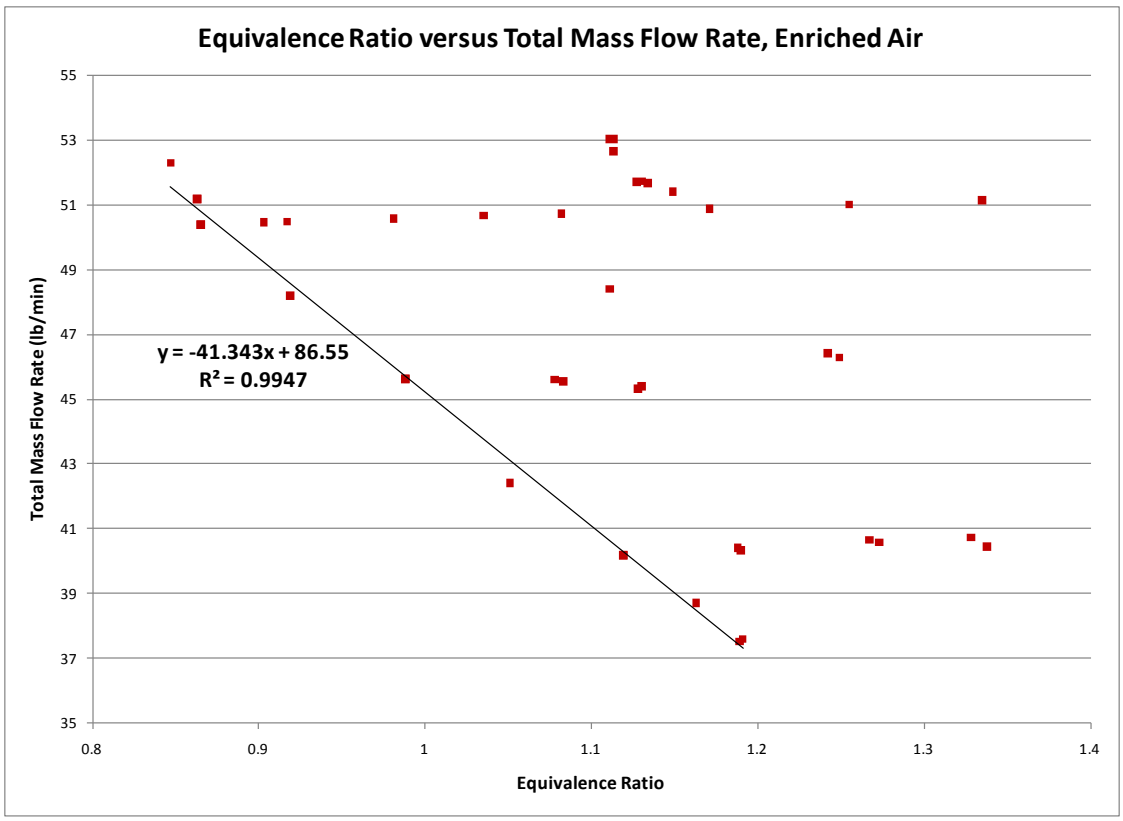

Figure 8. Operational space for 3 in diameter RDE running on enriched air[11]

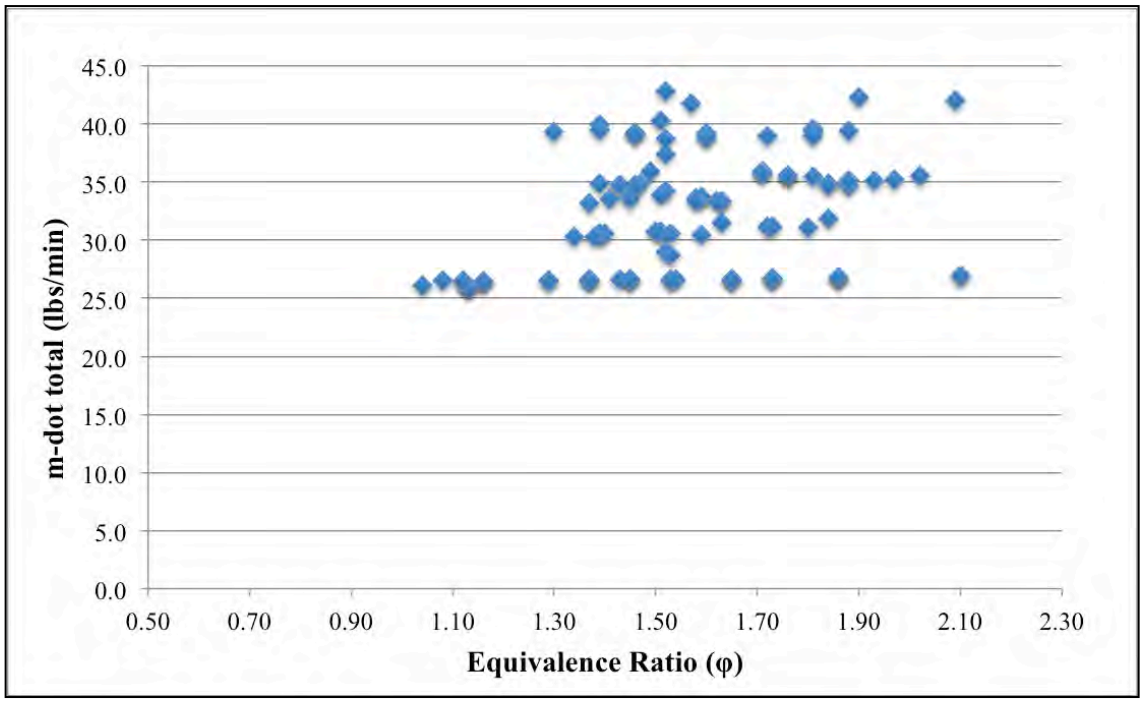

Figure 9. Operational space for 3 in diameter RDE running on standard air[12]

In both cases, runs had to meet two criteria to be deemed successful. First, the engine had to successfully detonate for a full 1s run time, and second, the test had to be repeated successfully three successive times. In both regimes, a linear lower limit of operation was found.

Data analysis techniques and error calculations were also refined during the testing of the 3 in RDE. Russo[11] developed and validated a time of flight code in Matlab to calculate wave speeds. The code calculates an average of the raw pressure data and searches for pressure peaks. Time between pressure peaks coupled with the detonation channel dimensions yield detonation wave speeds. Also calculated in the code is the error in the wave speed calculations. All error calculations were of the same form for this research since the same instrumentation was used.

CHAPTER 3. DESIGN AN DEVLOPMENT OF NEW 6IN RDE

3.1 Existing Detonation Engine Research Facility

Experiments were performed in Air Force Research Lab's (AFRL) Detonation Engine Research Facility (DERF). The DERF performs detonation engine research on both PDEs and RDEs. All support equipment and computers for testing were provided by the DERF and controlled remotely.

Various methods of data collection were used in this research. Visual data (standard speed and high-speed video) was collected via cameras installed within the DERF test cell. Low and high-speed pressure data was collected using a *LabView*® program. The low speed data collected includes upstream (of the air sonic nozzle) static air pressure, downstream (of the air sonic nozzle) static air pressure, upstream (of the hydrogen sonic nozzle) static hydrogen pressure, downstream (of the hydrogen sonic nozzle) static hydrogen pressure, fuel manifold pressure, and air manifold pressure. High-speed data was collected from pressure transducers installed in the RDE.

All systems for the RDE were controlled remotely from inside a control room. The RDE firing system is also housed in the control room. The control panel supplies power to the firing systems including the pre-detonator, fuel, and air (see Fig. 20). The control program sends various operational signals (e.g. open oxygen pre-detonator valve). If the RDE system does not have power, it will not run regardless of what the control computer is commanding.

3.2 Engine Design and Development

The DERF in AFRL already houses two RDE rigs; a 3in Pratt and Whitney developed RDE and a Boeing Corporation developed RDE. The RDEs' design cannot be published. This includes any specification on injection or mixing. Another drawback of the two rigs is that the engines were not designed to be modular. These two factors created a need in RDE experimental research.

A new RDE, designed by the author, was developed as an open-source design with simplicity and modularity in mind. Bykovskii[3] showed that an annular cylinder (as shown in Fig. 4) with proper width is a suitable detonation channel for nearly all cases.[3] The new RDE was designed around a simple detonation channel; with placement of the reactant plenums to the side and bottom of the channel. The oxidizer and fuel injection jets were positioned with the intent to promote a homogenous mixture in the detonation channel. Impinging jets should cause turbulence and result in better mixing than parallel jets. The oxidizer enters in the inward radial direction because of its much larger mass flow rate than fuel mass flow rate across all equivalence ratios. The fuel flows in the axial direction as illustrated in Fig. 10.

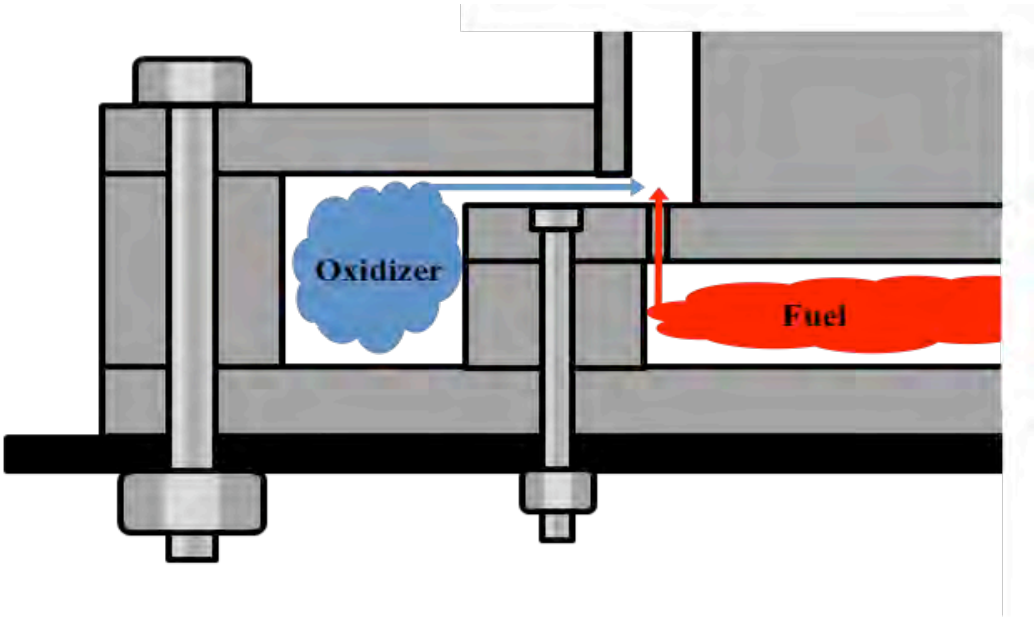

Figure 10. Modular RDE cutaway sketch with injection depicted

The high momentum of the oxidizer allows it to enter the channel, entrain fuel, and contact the center body between detonation waves. Contacting the center body should again promote a homogenous mixture of fuel and oxidizer in the detonation channel by causing turbulence.

The fuel and oxidizer mix in the detonation channel. While premixed reactants are ideal and would negate any mixing issues, a premixed plenum is dangerous since detonations can travel back into an isolated premixture plenum, creating an explosive potential.

A main purpose for building the RDE was to have a platform on which the five critical variables of an RDE could easily be changed. The five critical variables are: oxidizer type, oxidizer injection geometry, fuel type, fuel injection geometry, and detonation channel width. It was desired that the five variables could be changed independently. Oxidizer type and fuel type are determined by what is fed into the

respective plenums. Oxidizer injection geometry, fuel injection geometry, and detonation channel width are set by parts of the engine shown in Fig. 11.

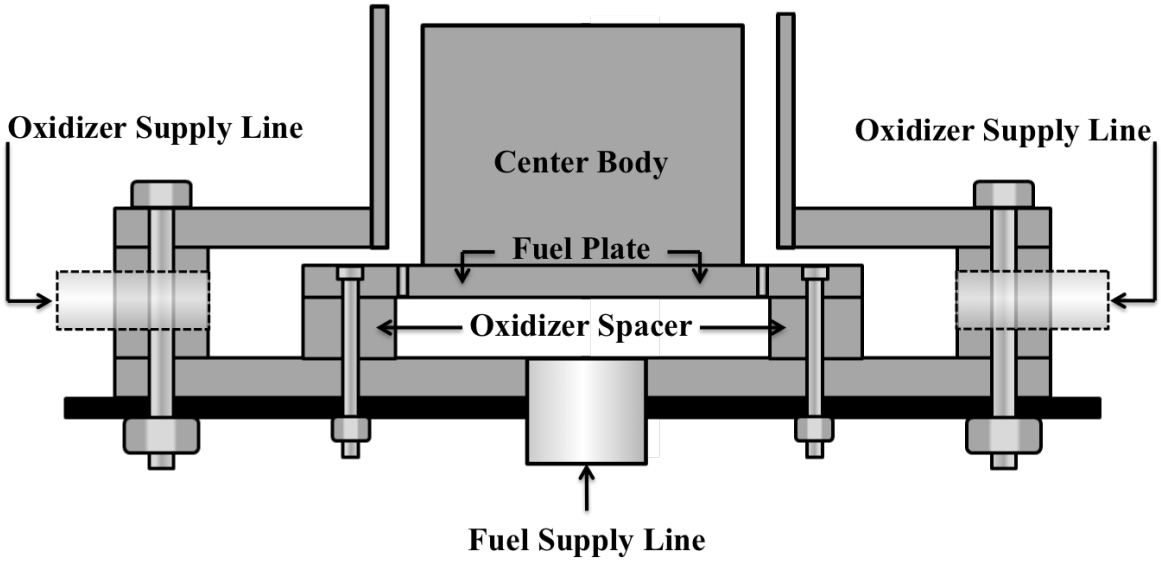

Figure 11. Modular RDE cutaway sketch with critical variable pieces labeled

Changing the height of the oxidizer spacer varies oxidizer injection geometry. Oxidizer injection geometry also depends on fuel plate thickness. A constant fuel plate thickness of 0.5in was used, and a spacer height of 1.125 in thickness was installed. The spacer resulted in a jet slot of 0.125 in. Fuel injection geometry depends on the design of the installed fuel plate. Experimentation included a fuel plate with 80, 0.1 in diameter holes arranged in a 5.96 in diameter circle. Detonation channel width is set by the outer diameter of the center body. Tests used a center body with a 5.46 in outer diameter, which results in a detonation channel width of 0.3 in. Figure 12 depicts the injection and detonation channel geometry.

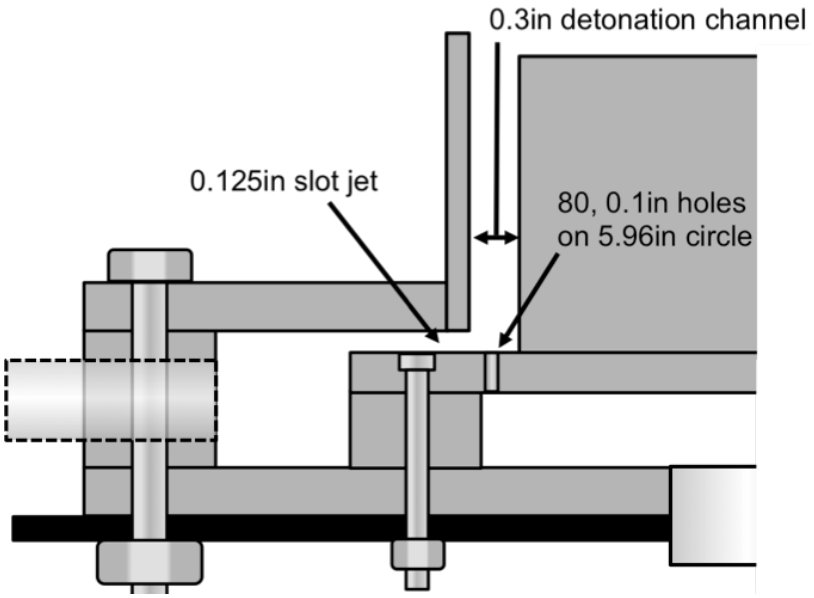

Figure 12. Injection and center body geometry

3.3 Engine Construction

CAD drawings of the RDE were made after the general design had been completed. The drawings can be found in Appendix A. The RDE is comprised of seven primary parts: a bottom plate, oxidizer main ring, oxidizer spacer, fuel plate, top ring, outer body, and center body. Figure 13 shows the assembly drawing of the RDE with all 7 pieces labeled.

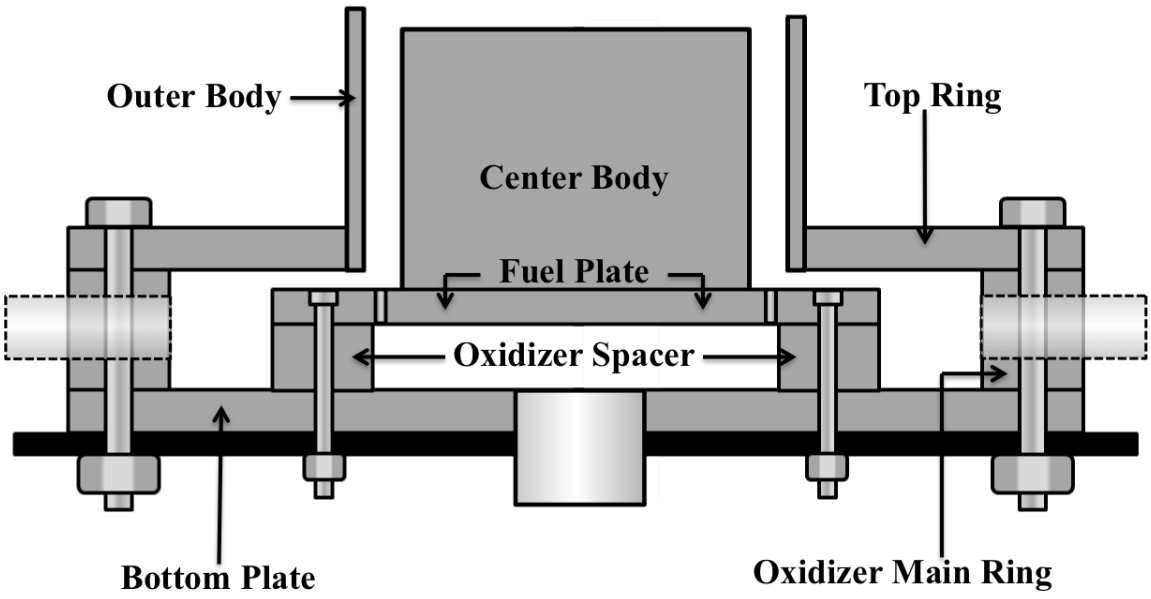

Figure 13. Assembly drawing of new 6 in RDE

The oxidizer plenum is supplied via five side ports in the oxidizer main ring. The fuel plenum is supplied via a single port in the center of the bottom plate. All pieces are of hoop or disk design. The hoop and disk design allows easy interchange and modification of parts. All parts were fabricated from metal plate stock with the exception of the center body and outer body. The outer body and center body were fabricated from 160 schedule metal pipe.

The RDE is constructed from two different types of material. Parts in contact with the detonation channel are made of stainless steel, chosen for its high melting temperature. Although the RDE is only run for one second without any type of thermal management system, temperatures are high enough such that aluminum would melt. Parts made of stainless steel include the center body, outer body, top ring, and fuel plate. The other parts (bottom plate, oxidizer main ring, and oxidizer spacer) are made from 7075 aluminum.

3.4 Engine Installation

The RDE was installed in the RDE test area of the DERF. A separate steel test stand was constructed for the RDE and securely attached to the concrete. The test stand allowed for direct attachment of the RDE via thru holes in the tabletop. Nuts on the bottom of the tabletop, as shown in Fig. 14, securely hold the RDE in place.

Figure 14. Bottom of RDE test stand showing attachment and fuel supply line

Structural analysis of the RDE revealed the limiting factor to be the attachment bolts. SAE grade 3, 0.5 inch bolts limit oxidizer plenum pressure to 600 psi maximum. Previous work at AFRL showed this maximum allowable pressure to be well above what would be needed. Testing, discussed later, resulted in oxidizer plenum pressures of approximately 85 psi.

Figures 15 through 18 show buildup of the RDE on the test stand.

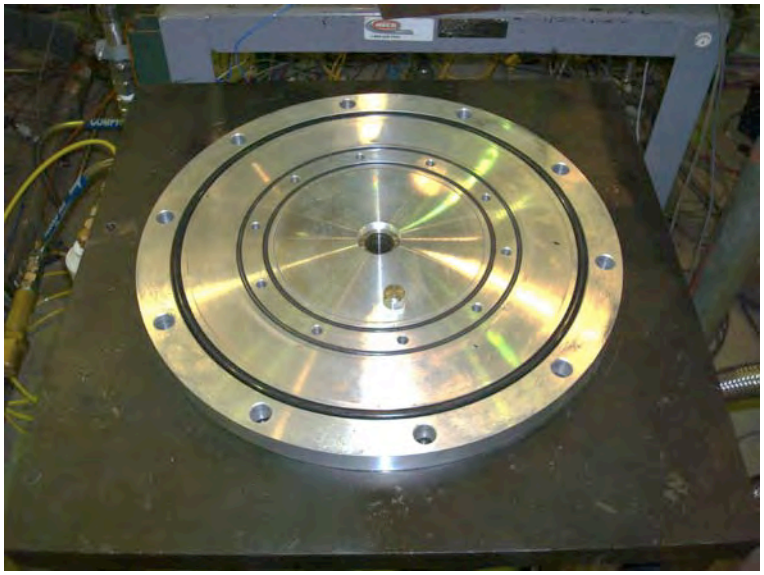

Figure 15. Bottom plate on test stand

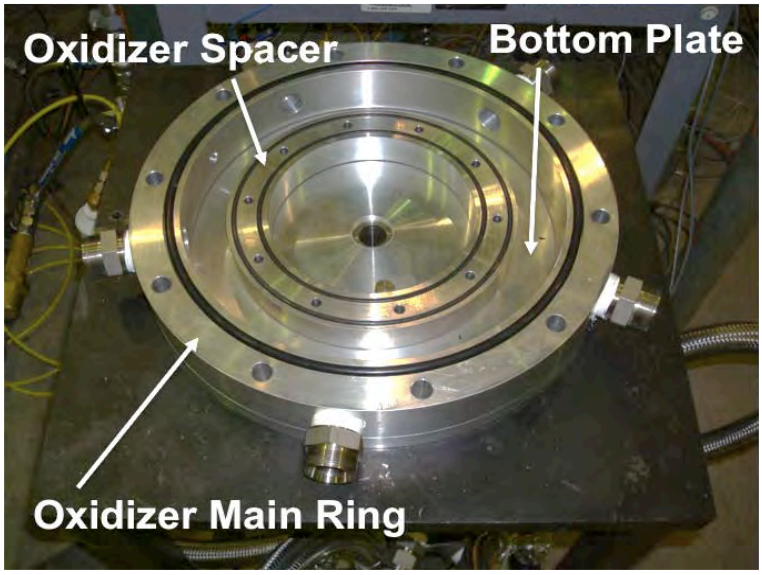

Figure 16. RDE with bottom plate, oxidizer spacer, and oxidizer main ring installed

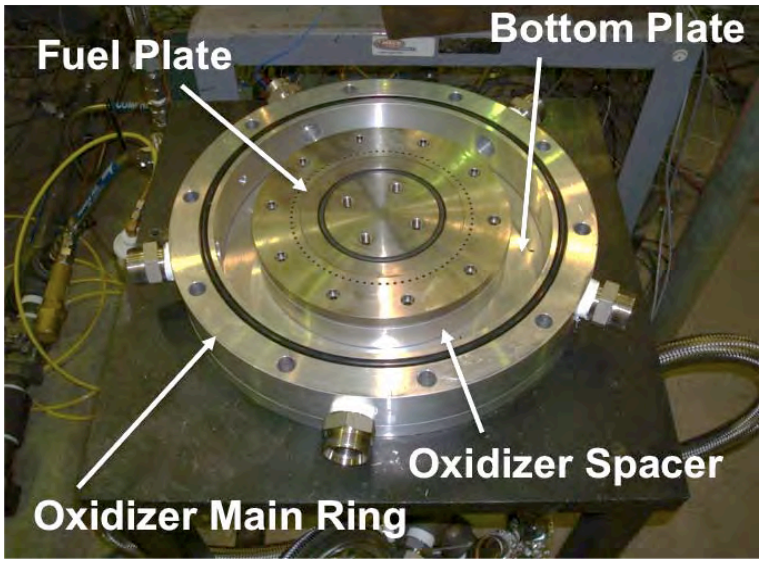

Figure 17. RDE with bottom plate, oxidizer spacer, oxidizer main ring, and fuel plate installed

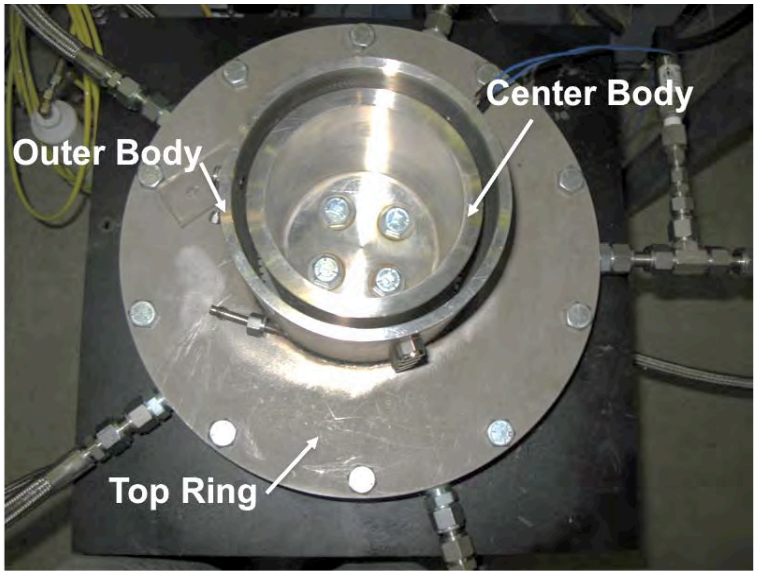

Figure 18 Top view of RDE completely installed

Fuel and oxidizer supply lines were installed after the RDE was in place. A 0.75 in main line supplies fuel to the RDE (seen in Fig. 14). A 1.5 in main line supplies oxidizer to the RDE. The 1.5in line was installed after the discovery that a 0.75 in line choked the flow. The larger diameter line caused the oxidizer to be choked at the

detonation channel inlet. Figure 19 shows the installed supply lines installed and the fuel flow path (marked in red) and oxidizer flow path (marked in blue).

Figure 19. Highlighted oxidizer and fuel supply lines with flow path highlighted

Figure 20 shows a schematic of the fuel and oxidizer delivery systems in their entirety. Two separate fast-acting pneumatic valves control fuel and oxidizer flow to the RDE. Dome-loaded pressure regulators and sonic nozzles control the mass flow rates of the reactants.

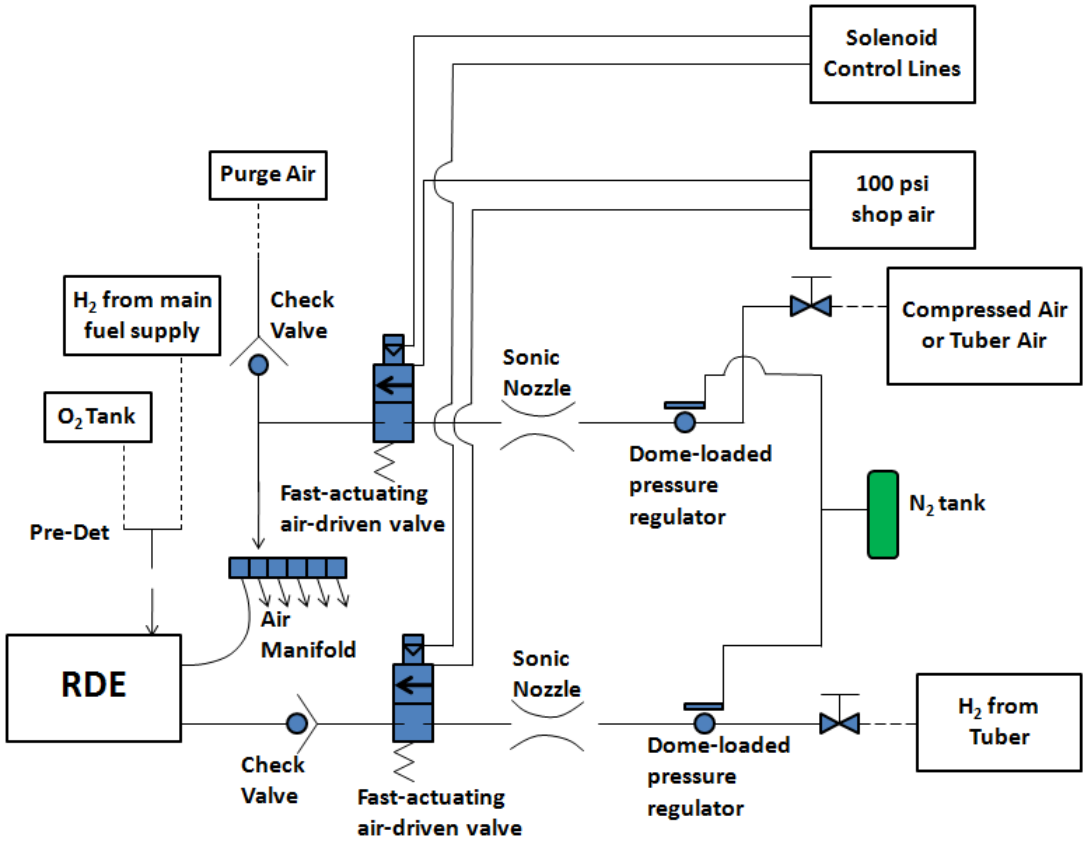

Figure 20. Schematic of oxidizer and fuel delivery systems[10]

As can be seen in texts such as reference #13, mass flow can be calculated using,

$$\dot{m} = \frac{Ap_t}{\sqrt{T_t}}\sqrt{\frac{\gamma}{R}}M\left(1+\frac{\gamma-1}{2}M^2\right)^{-[(\gamma+1)/2(\gamma-1)]} \quad (1)$$

Sonic nozzles with known diameters are installed in both the oxidizer and fuel supply lines. Thus A is known and M = 1 in Eq. 3. T_t is approximately constant at 68°F. γ is 1.4. Adjustment of p_t varies mass flow. A choked condition in the sonic nozzle is verified by static pressure transducers upstream and downstream of each sonic nozzle.

Air for testing can be supplied from two different sources. Tuber trailers can supply air with either 25% or 23% oxygen. Air from a compressor located behind the DERF supplies standard air with 21% oxygen. Hydrogen is supplied from a tuber trailer.

3.5 Engine Ignition

In order to start a detonation in the detonation channel, a detonation is initiated tangentially to the flow via a spark plug initiated pre-detonator. Figure 21 shows the pre-detonator installed on the RDE with all parts labeled. Pure oxygen and hydrogen flow into a 2.5in long, 1/4in diameter tube that is welded into the sidewall of the outerbody. The mixture is ignited, deflagration to detonation transition occurs, and the detonation is ejected into the RDE detonation channel.

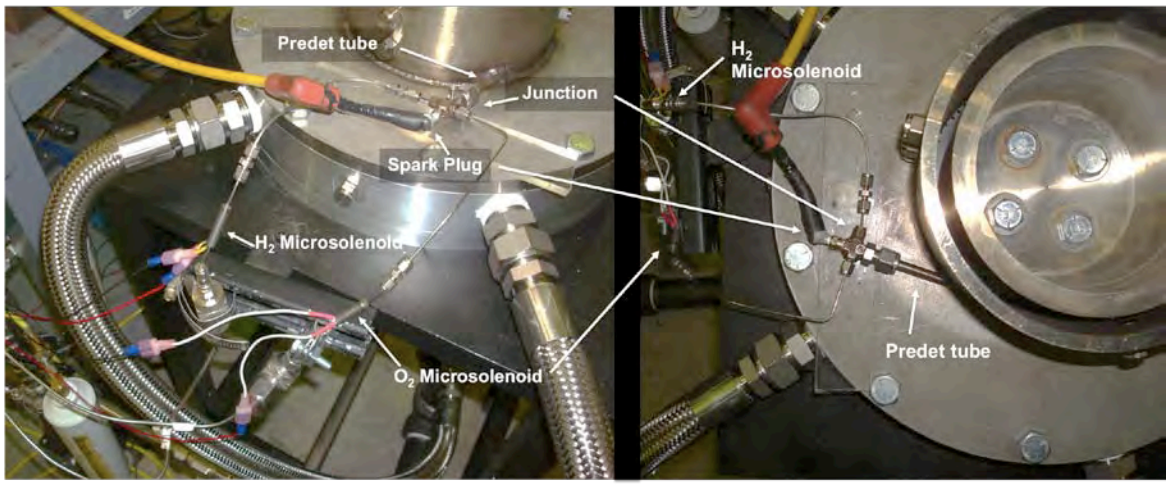

Figure 21. Side and top views of predetonator installed on RDE

3.6 Instrumentation and Data Collection

The RDE was designed to be flexible in placement and type of instrumentation. Three circumferential stations (120° offset) with four ports arranged vertically provide a variety of measurement locations. Figure 22 shows the ports in the outer body of the engine.

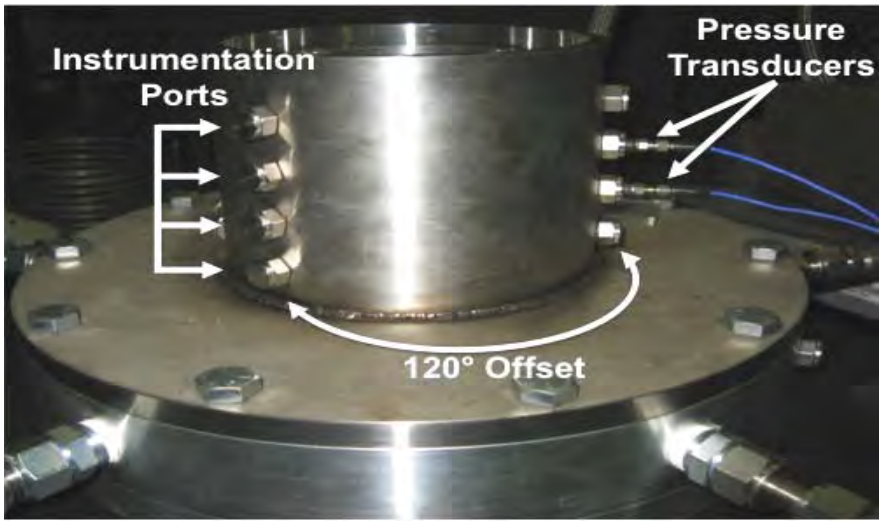

Figure 22. Instrumentation ports on the RDE outer body

For this research, PCB® Piezoelectric Dynamic Pressure Transducers were arranged in a vertical stack as shown in Fig. 22. Stacking the pressure transducers allowed for consistent detection of the detonation wave. High-speed pressure transducers spike when a large pressure gradient is present (i.e., a detonation wave). A transducer rise time of less than 1μs allows precise temporal measurement when a detonation wave passes. The transducer data a serve dual purpose: indicating a detonation wave is present and allowing calculation of the detonation wave speed. High-speed PCB® pressure transducer data was collected at 1MHz beginning with the "fire" command sent from the control computer.

Flow visualization was also used in testing. Standard speed and high-speed cameras gave visual indication of the presence of detonation. A high-speed camera was used with the setup shown in Fig. 23 to allow visual access into the detonation channel.

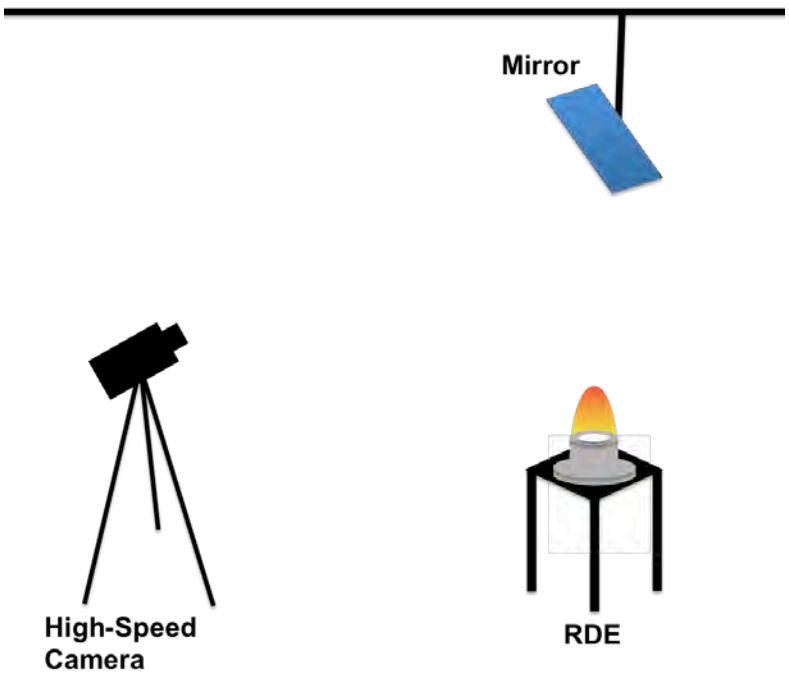

Figure 23. Visual access to detonation channel

Video from the high-speed camera was captured and analyzed to distinguish between deflagration and detonation events. A deflagration event would not be visible in the high-speed video, while a detonation event would appear as a distinct white front traveling around the detonation channel. Figure 24 shows a 10 frame, high-speed video sequence of a successful detonation event. High-speed video in Fig. 24 was collected at 31 kfps, 6 μs exposure time, and at a resolution of 128x128 pixels. Ten frames for one revolution of the detonation wave correspond to a wave speed of 1515 m/s.

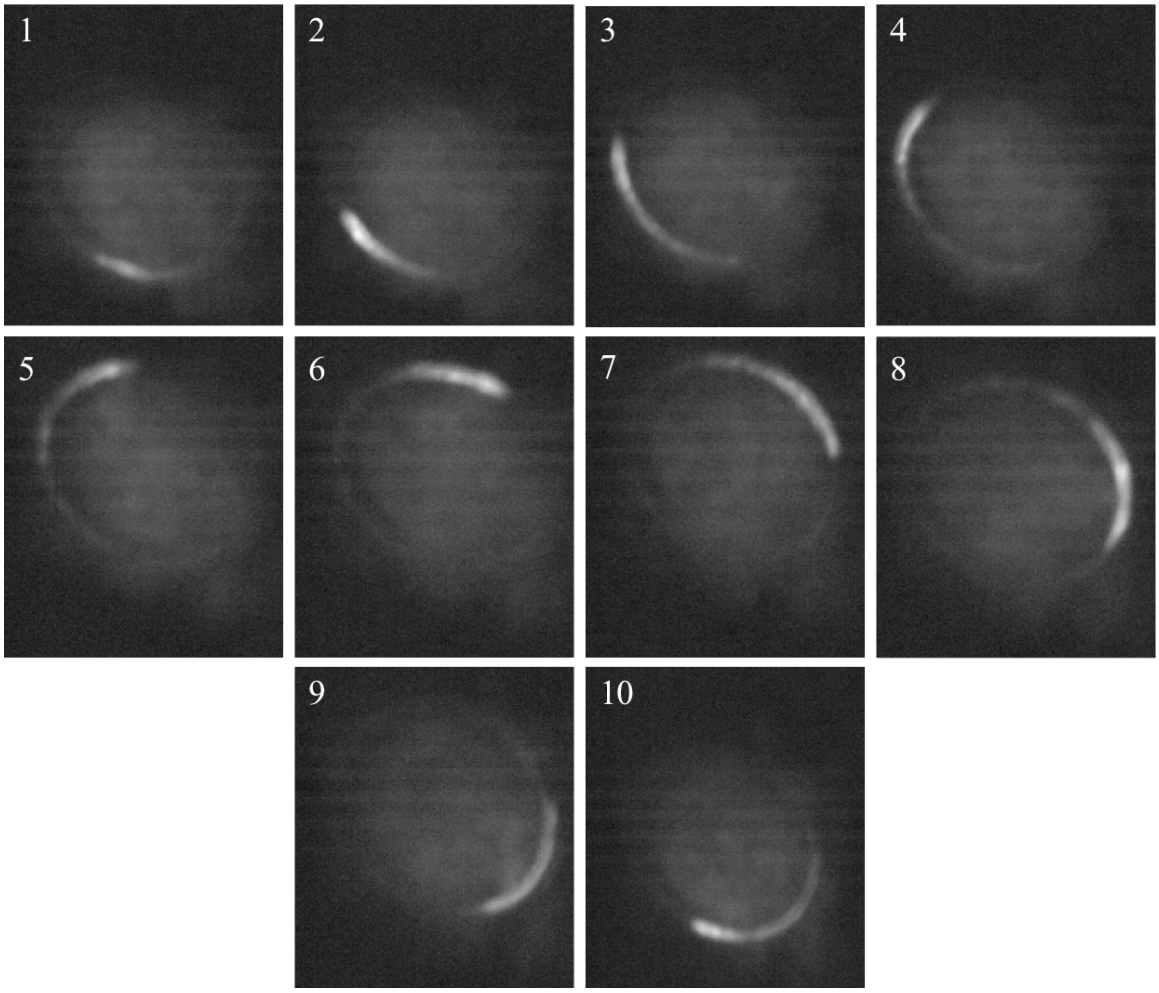

Figure 24. Ten frame sequence of detonation wave traveling around detonation channel

Video from a standard speed camera (30 fps) was also used to indicate occurrence of a detonation event. Figures 25 and 26, respectively, show a deflagration event and a detonation event. A deflagration event appears as a tall flame, approximately nine feet in height for this build. A detonation event appears as a shorter dome shaped flame, approximately one to two feet in height.

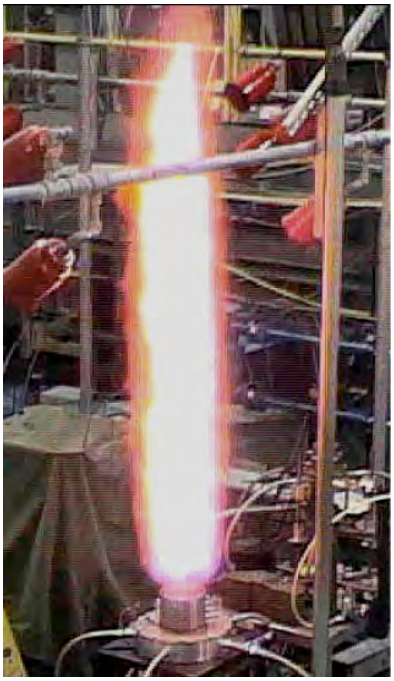

Figure 25. Deflagration flame captured with standard speed camera

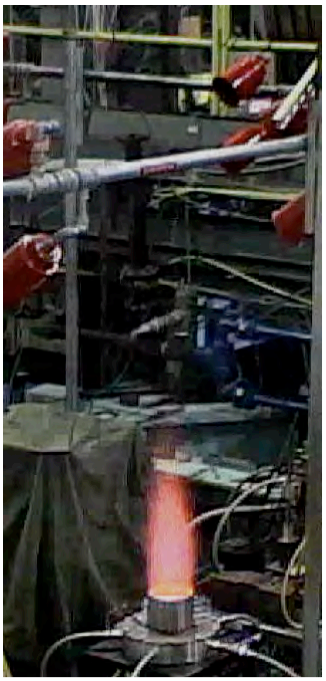

Figure 26. Detonation flame captured with standard speed camera

3.7 Successful Run Criteria

A primary goal of this work was to map the operational space for the new 6 in RDE. In order to confidently determine whether detonation had occurred for a given total mass flow and equivalence ratio, success criteria were established. High-speed PCB® pressure transducer data and high-speed video footage were used to verify detonation. Standard speed video and auditory observations were only used as qualitative indications of detonation occurrence.

Runs were deemed successful if the engine ran and detonations occurred for one second. A full 1 s run was verified by the high-speed pressure data and high-speed video. The high-speed data appeared as in Fig. 27, and the high-speed video appeared as in Fig. 24. Figure 28 shows an expanded view of the high-speed pressure data from Fig. 27. Each peak represents passage of the detonation wave.

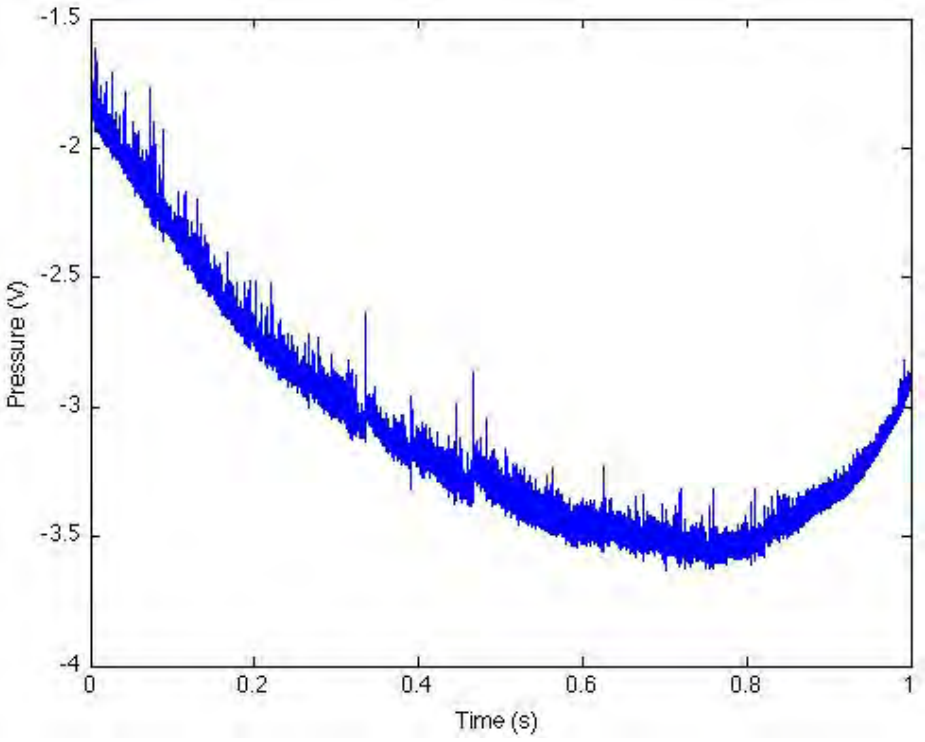

Figure 27. High speed pressure data from a successful run

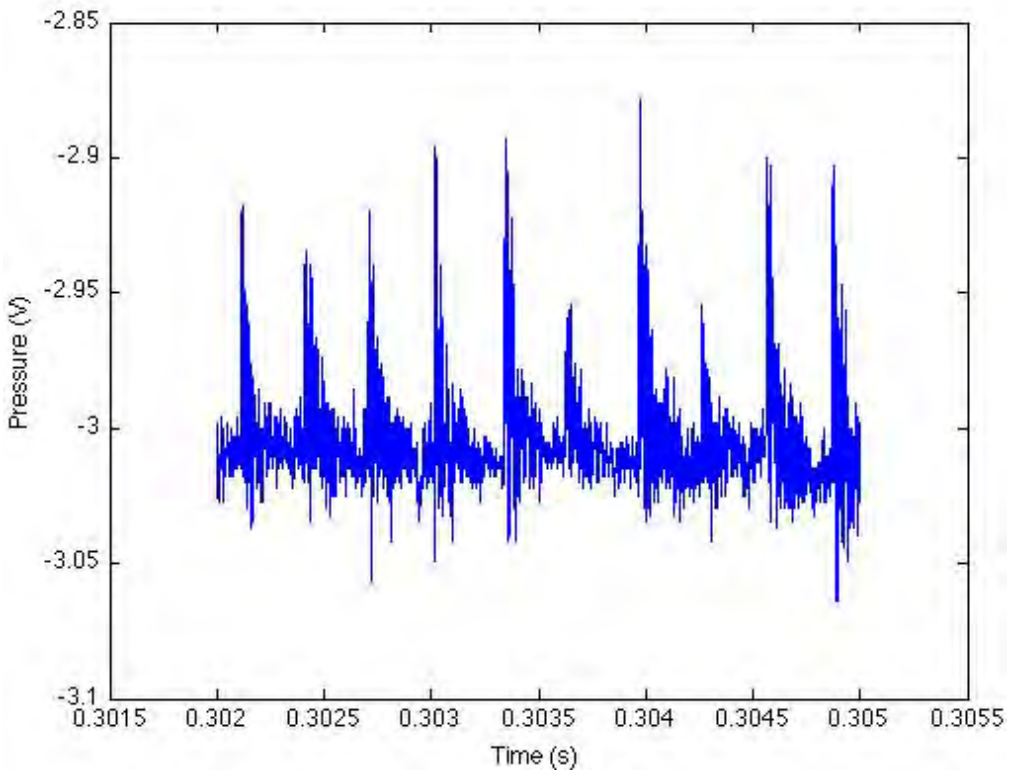

Figure 28 Zoomed in high-speed pressure data showing peaks from a successful run

The data in Fig. 27 show the thermal drift associated with a detonation event; the changing zero of the pressure spikes evidences thermal drift. The drift was an instrumentation characteristic and provided another indication of a successful run. Other qualitative observations of a successful run include a dome-shaped flame as in Fig. 26 and a distinct, high pitched screech. It should be noted that the high-speed pressure data and high-speed camera agreed on indicating successful detonations.

3.8 Data Reduction

Data reduction and error analysis techniques previously developed[11] and validated were used as a foundation for data reduction in this research (see Appendix B for code).

The time-of-flight code finds the peaks in the high-speed pressure data and calculates the time between them. With the detonation channel dimensions known, the detonation velocity is then calculated according to,

$$V_{det} = \frac{combustion\ channel\ circumference}{time\ between\ pressure\ peaks} \quad (4)$$

For insight into code validation and sensitivity analysis see Russo's "Operational Characteristics of a Rotating Detonation Engine Using Hydrogen and Air"[11].

Small changes were made to the data reduction code for this application. The first change was the hold time, explained as follows. The time of flight code calculates an average pressure over the entire run time and finds peaks that lay more than one standard deviation above the average. A hold time to find another peak is initiated once a peak is found. This prevents double counting a peak. For this application, a hold time was chosen related to V_{CJ}. For hydrogen and air, V_{CJ} is theoretically equal to 1950 m/s. At that speed, there are 248 μs between wave passes in a 6in diameter RDE. Therefore a hold time of 240 μs was used. Figure 29 depicts how the hold time operates.

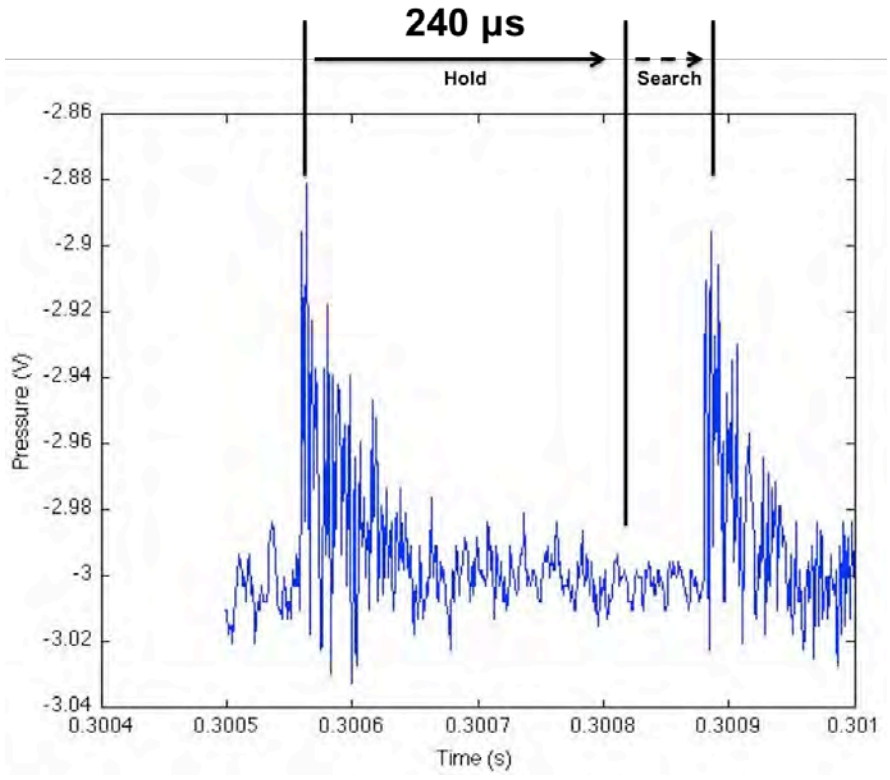

Figure 29. Visualization of data reduction code hold time between pressure peaks

The data reduction code was also adjusted to remove an aliasing error. Prior research[11] deemed four points must lay at least one standard deviation above the mean to be counted as a pressure peak. This constraint (4 points) seemed to suggest that the engine had two primary velocities of operation, one a supersonic speed and two a subsonic speed approximately half the value of the supersonic speed. A sensitivity analysis revealed that as the required number of points above the threshold is reduced to two, the subsonic combustion band disappears. Figures 30 through 32 show the disappearance of the subsonic velocity band.

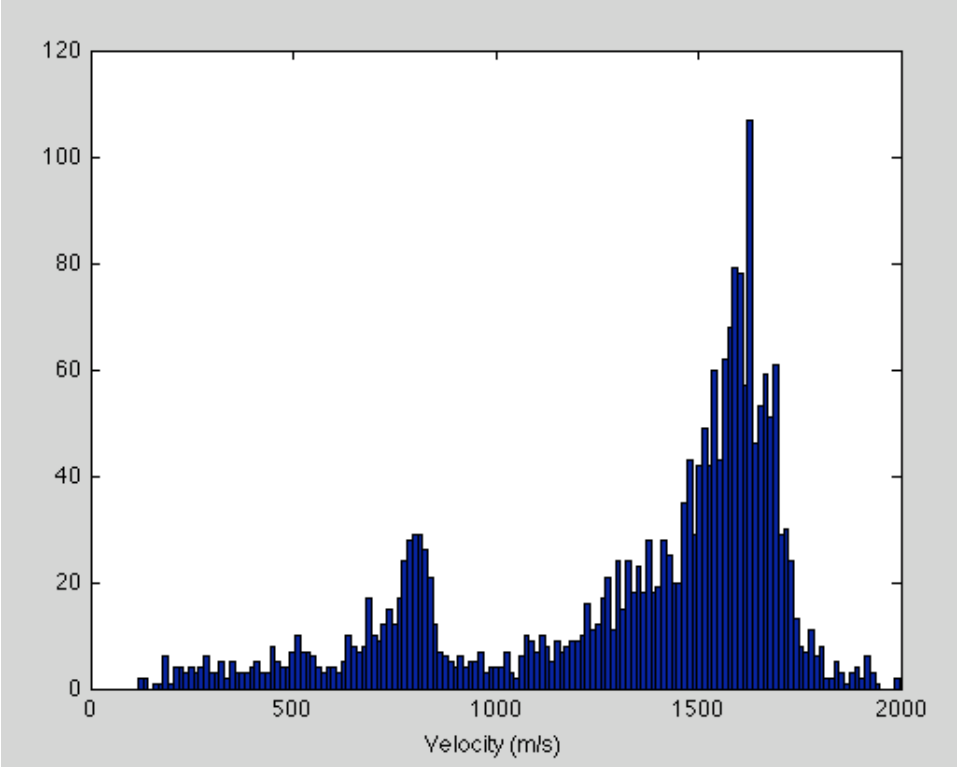

Figure 30. Velocity histogram for 4 points above threshold to determine pressure peak

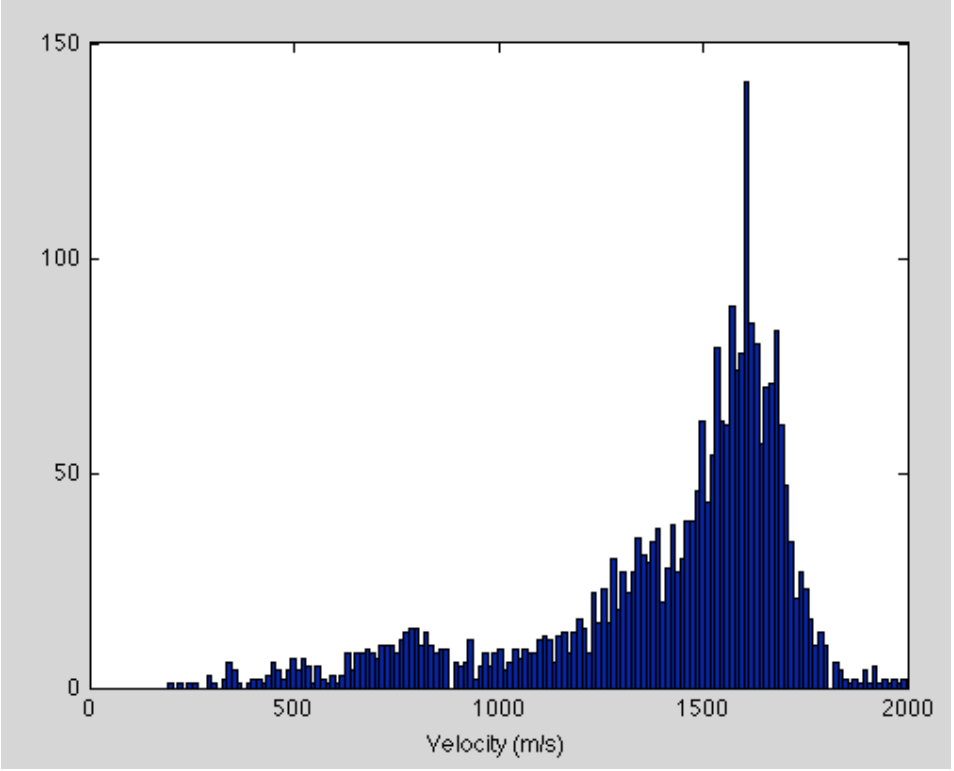

Figure 31. Velocity histogram for 3 points above threshold to determine pressure peak

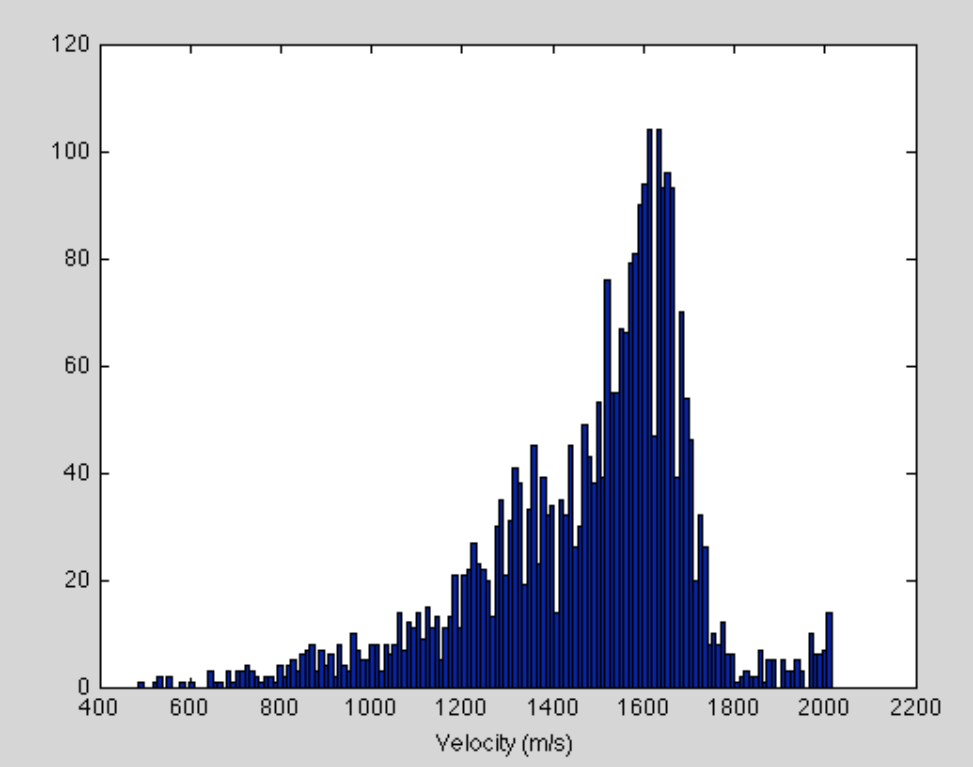

Figure 32. Velocity histogram for 2 points above threshold to determine pressure peak

Two points above the threshold value was used for all data analysis contained in this report. Two points produced data in accordance with speeds seen in the high-speed video.

Besides determining if detonation had occurred, high-speed video gave insight into the variability of the wave speed as it traveled around the detonation channel. High-speed video taken at 50 kfps was analyzed using a new technique where a compass was overlaid onto the video as shown in Fig. 33**.** Blue circles mark the three sets of instrumentation ports. The pre-detonator position is marked with a red circle.

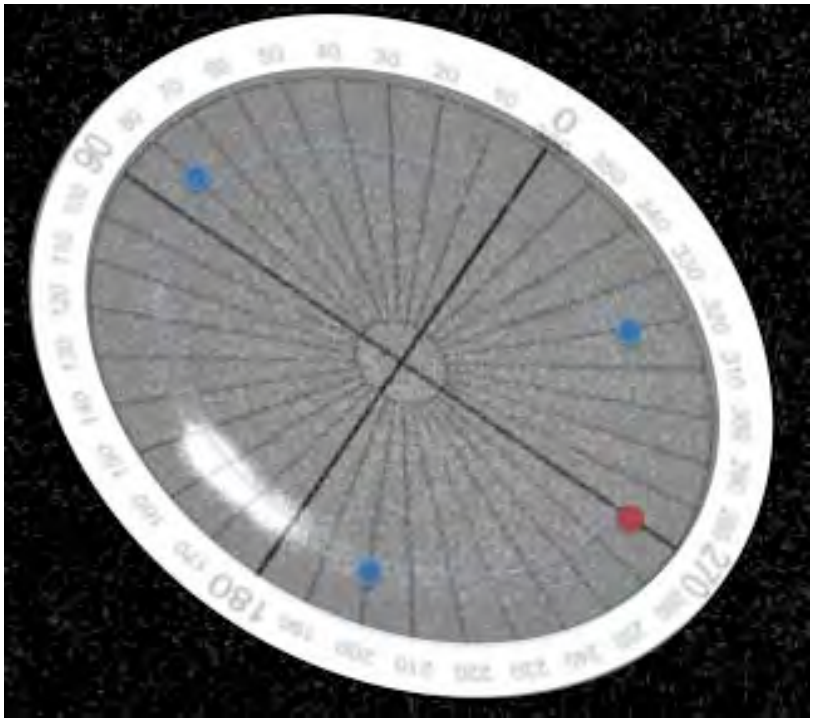

Figure 33. High-speed video with analysis compass overlaid

The polar position of the detonation front was noted for each frame. The distance traveled between frames was then calculated using the known annulus outer radius (3.03 in). The wave velocity was calculated knowing the time between successive frames and distance traveled. Time was known from the camera speed (50 kfps) with zero-time corresponding to the first frame analyzed. A graph plotting wave speed versus time was ultimately generated. Also noted in the wave speed plot was the time at which the detonation wave passed an instrumentation port or the predetonator port (see Fig. 39).

CHAPTER 4. RESULTS AND DISCUSSION

4.1 Overview

Beyond the development and installation of the new RDE, this research also included an investigation into the RDE operational space and wave speeds. The operational parameters varied were the total mass flow rate and equivalence ratio. Detonation velocity and high-speed video footage were used to validate the success of the run. High-speed video was also used to track the variation of wave speed around the detonation channel.

4.2 Operational Space

Figure 34 shows the operational space for the 6in RDE run on hydrogen and standard air (see Appendix C for raw data). Of interest was finding the bottom and left boundaries for successful operation. Successful operation was defined in section 3.7. The bottom boundary in Fig. 34 appears to be distinct, the left boundary less so. Further investigation revealed both boundaries to be a more distinct function of fuel mass flow rate and equivalence ratio, as shown in Fig. 35 (see Appendix D for raw data). The graph reveals a linear relationship for successful operation along the bottom operational boundary shown in Fig. 34.

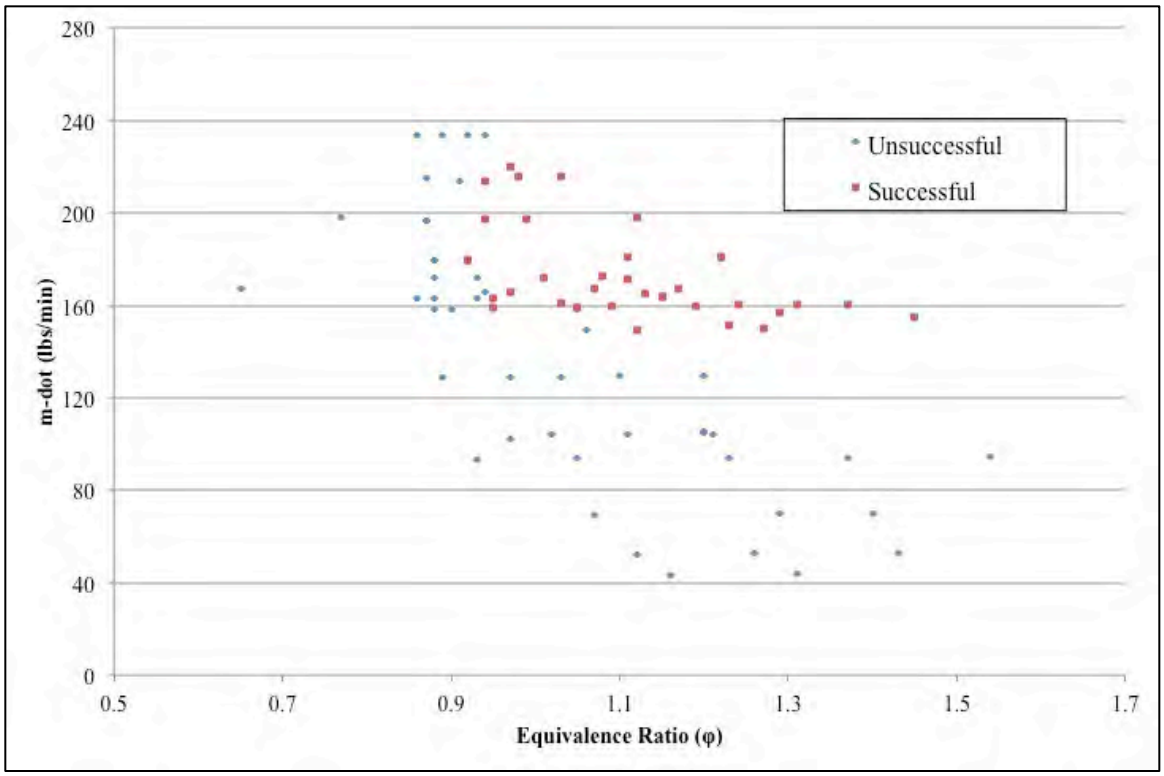

Figure 34. Operational space for RDE run on hydrogen and air

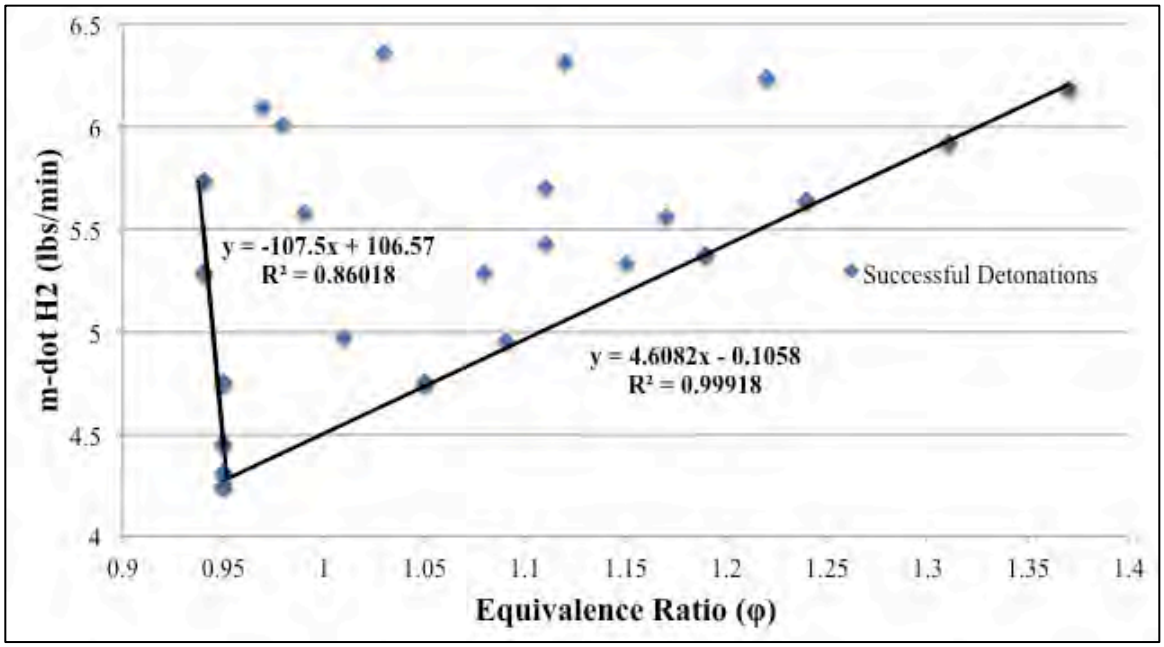

Figure 35. Operational space for RDE as a function of equivalence ratio and fuel flow

Fuel flow rate varied linearly between equivalence ratios of 0.95 and 1.4. The left operational boundary in Fig. 34 is depends on equivalence ratio. An equivalence ratio of approximately 0.94 is the minimum equivalence ratio that achieves successful operation.

4.3 Comparison to 3in RDE Operational Space

Comparisons between the 3in RDE and 6in RDE operational spaces were done to highlight similarities and differences between two RDEs of differing diameters. The first difference noted is that the operational space is not solely dependent on total mass flux. Figure 36 shows each RDE's successful operational space with total mass flux plotted against equivalence ratio.

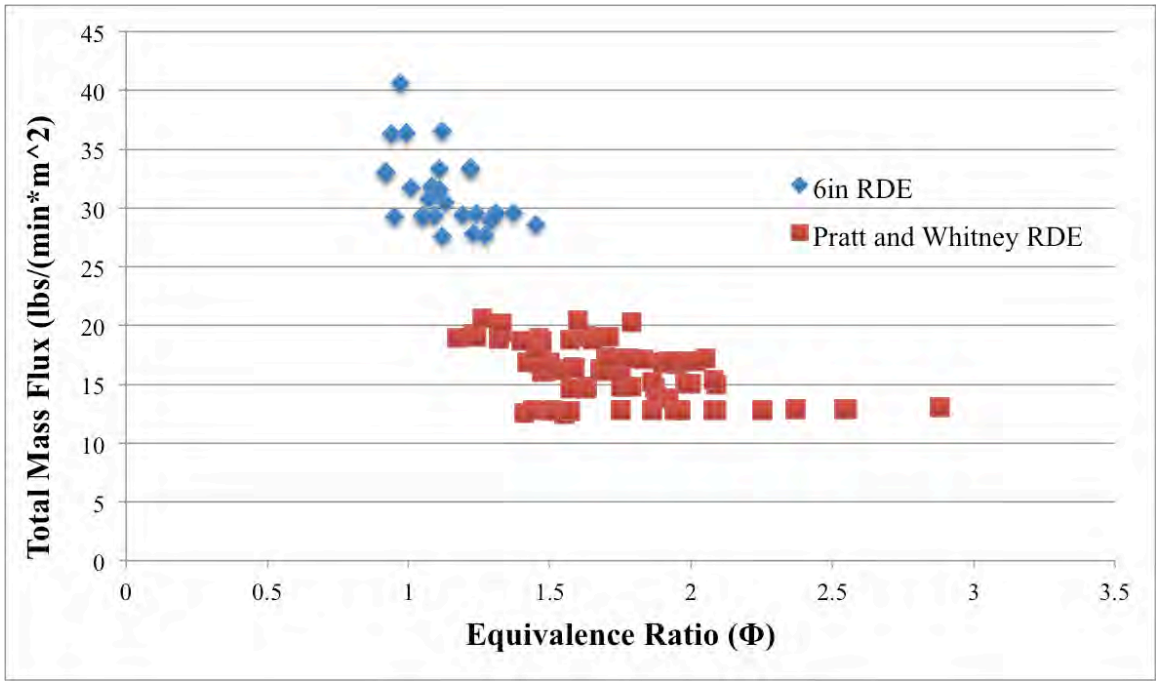

Figure 36. 6in and 3in RDE op space normalized by detonation channel area

One similarity between both RDEs (shown in Fig. 37) is the lower boundary of operation is a linear relationship between fuel mass flow rate and equivalence ratio.

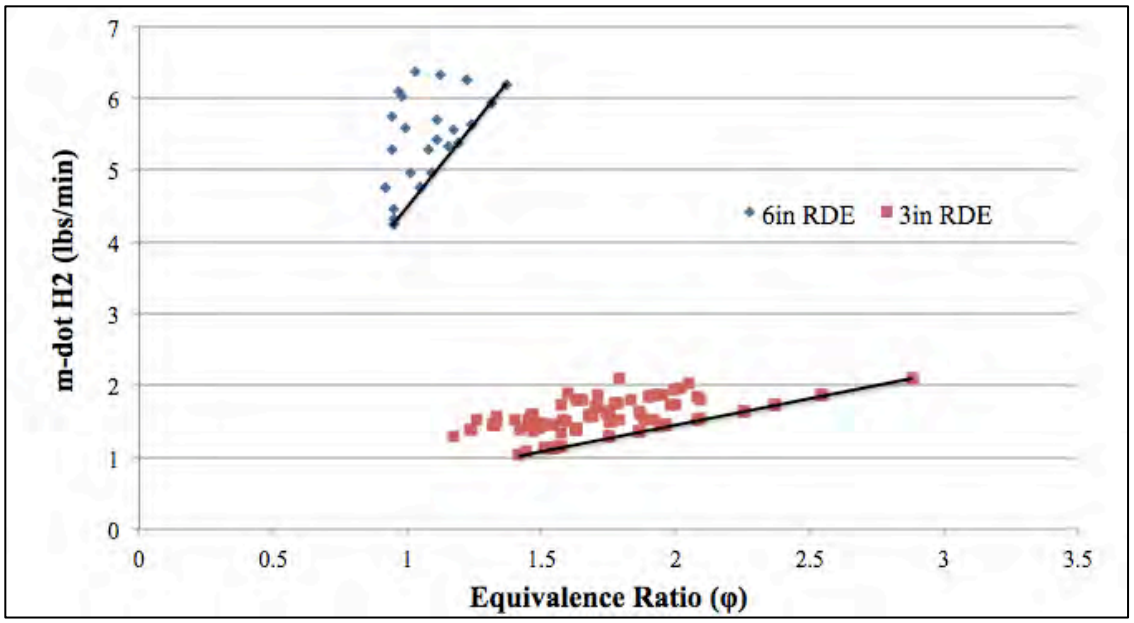

Figure 37. 6 in and 3 in RDE op space as a function of equivalence ratio and fuel flow

Definition of the left hand boundary differs between each RDE. The 6 in RDE depends on equivalence ratio alone while the 3 in RDE depends on both equivalence ratio and fuel flow rate.

Comparison of the two RDE operational spaces lends some insight into general RDE operation. In both cases, mapping fuel flow rate versus equivalence ratio best defines operating boundaries. It is hypothesized operational differences seen in Fig. 37 between the two RDEs, are a function of their respective injection schemes. Due to proprietary limitations design comparisons are prohibited.

4.4 Wave Velocity

Detonation wave speeds for the 6 in RDE were higher than those previously observed[3, 11, 12], but below V_{CJ} of 1950 m/s. The 3 in RDE wave speeds varied between 1200 m/s and 1400 m/s.[11] Six inch RDE wave speeds varied between 1400 m/s and 1550

m/s. It was found wave speed is related to the total mass flow rate for the 6 in RDE. Figure 38 shows the variation of wave speed with total (fuel+air) mass flow rate. It reveals that as total mass flow rate increases from 160 lbs/min to 220 lbs/min, wave speed increases approximately linearly from 1410 m/s to 1560 m/s.

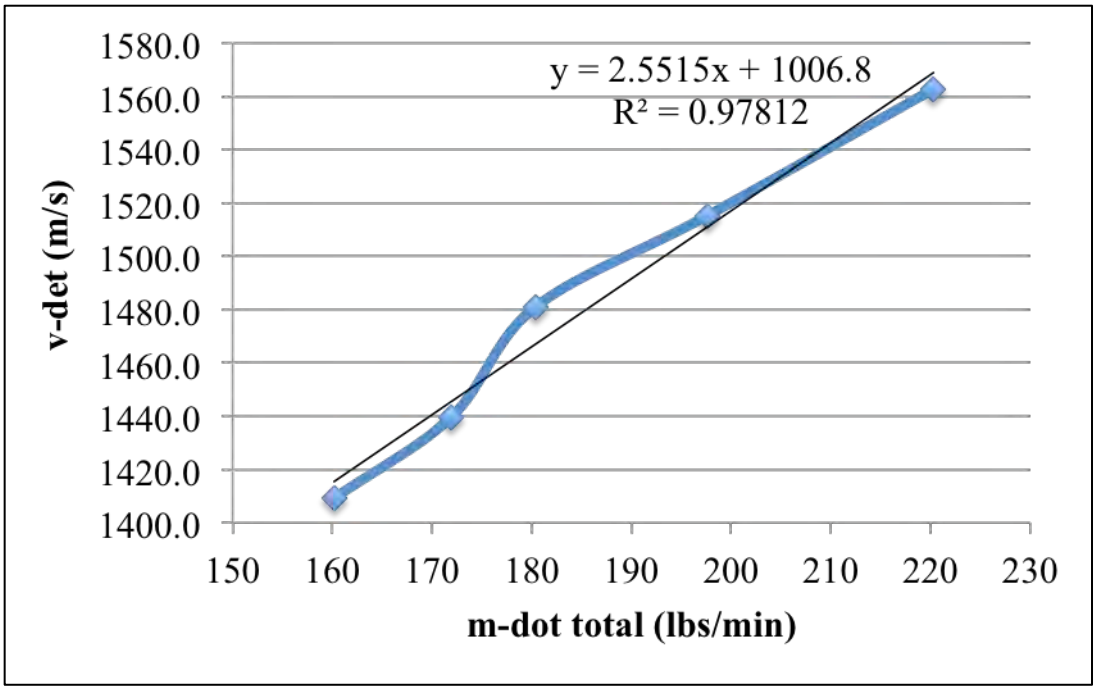

Figure 38. Wave speed plotted as function of total mass flow rate

The wave speeds from Fig. 38 represent the average speed over an entire 1 s run (see Appendix E for data). Wave speed was found utilizing the time-of-flight code previously discussed. One outlier speed exists at $\dot{m}_{total}$ = 180 lbs/min. PCB data was only obtained for two runs of $\dot{m}_{total}$ = 180 lbs/min. It is believed v_{det} would fit the trend should more run data be procured. Future work should test the hypothesis.

Histograms for various runs appeared as in Fig. 39. The histograms revealed detonation wave speed is centered about the mode, but varies throughout a run. High-speed video analysis was done to determine why.

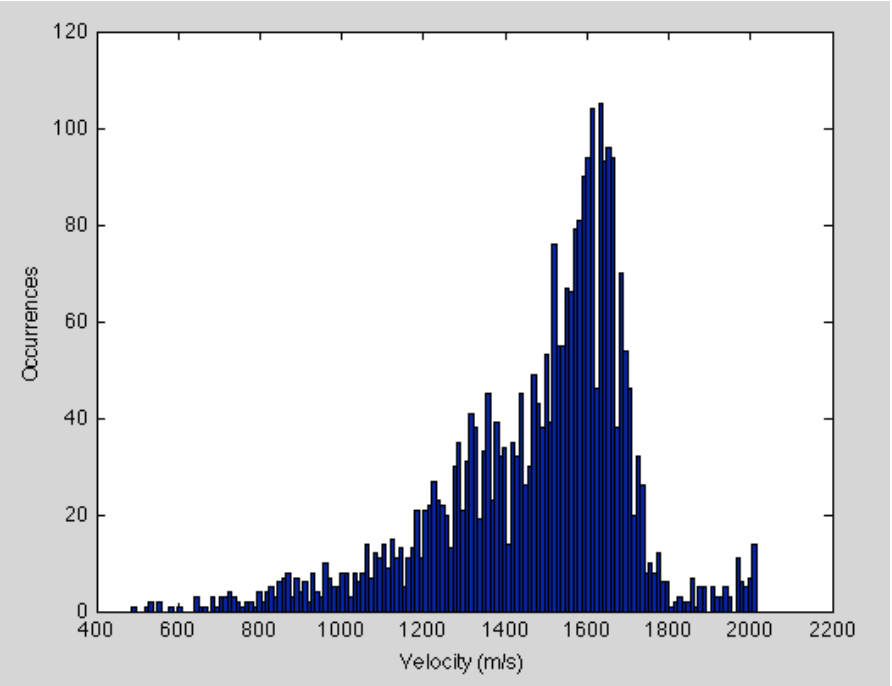

Figure 39. Histogram for 1 s run with $\dot{m}_{total}$ = 153.5 lbs/min and Φ = 1.09

High-speed video showed a large amount of unsteadiness throughout a run. General operation can be grouped into three modes, however; rotation, reversal, and bifurcation. In rotation, one detonation wave consistently travels around the detonation channel in one direction. Figure 24 shows a high-speed video frame sequence for the rotation mode of operation. In reversal mode, one detonation wave reverses its rotation direction. Figure 40 shows a reversal.

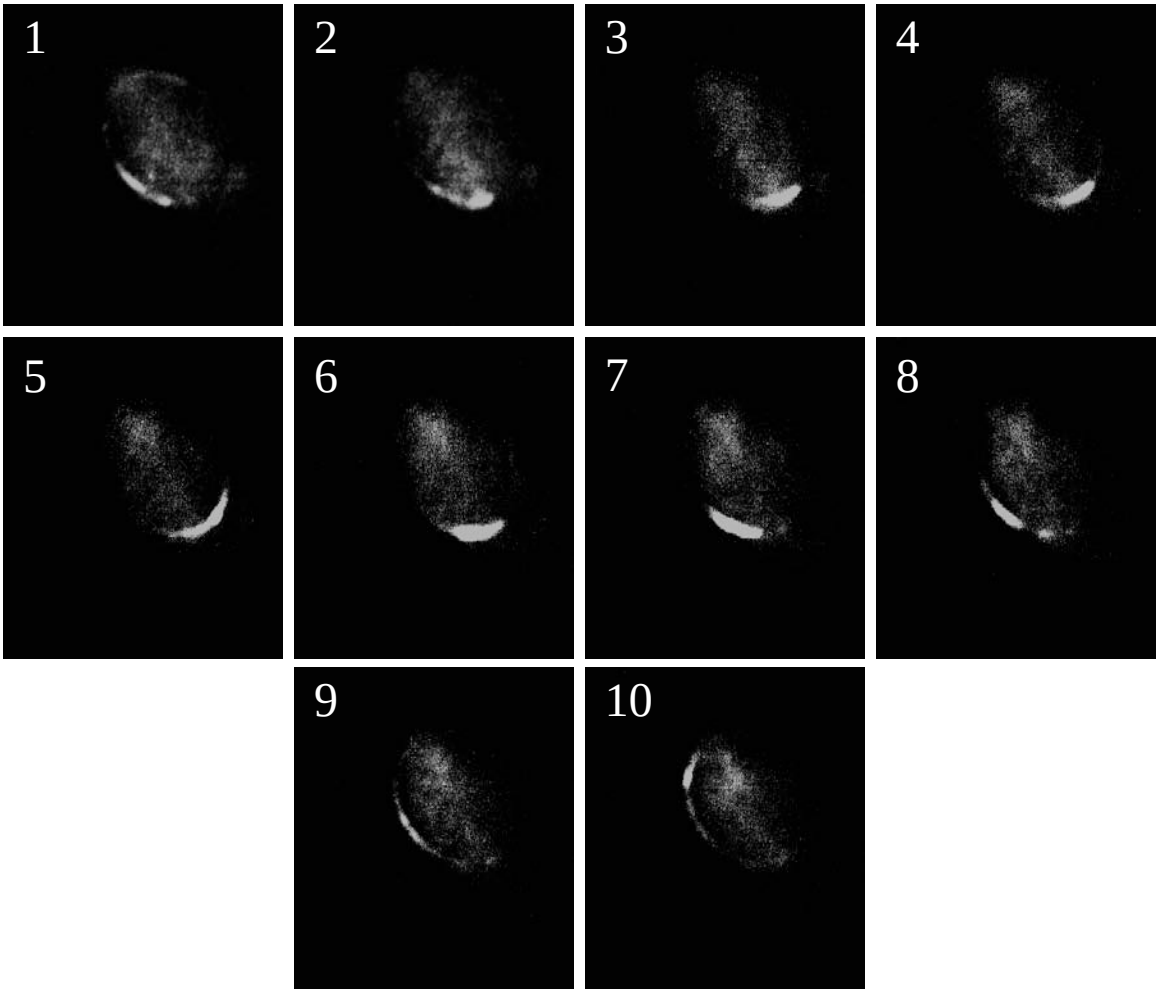

Figure 40. High-speed video showing reversal mode of operation

The third mode of operation, bifurcation, is characterized by formation of two detonation waves. This mode of operation is seen throughout the course of a run, but is consistently observed during engine ignition. Two detonation waves are produced traveling in opposite directions when the predetonator ignites the engine (see Fig. 41).

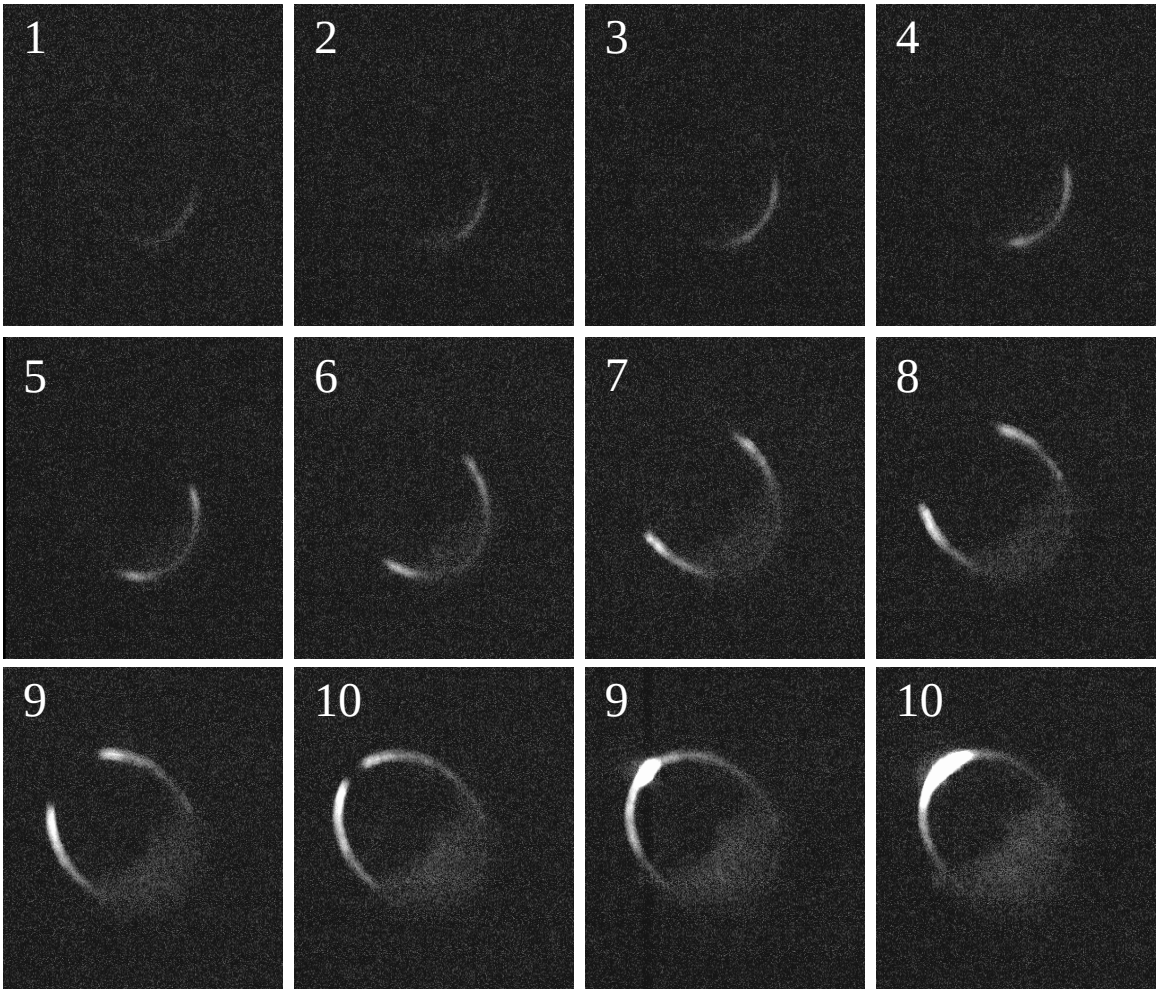

Figure 41. High-speed video showing bifurcation mode of operation

Throughout the analysis of the high-speed video it was noticed that the detonation front illuminates and/or reverses at primarily three points, approximately 120° offset, corresponding to the instrumentation ports. Figure 42 shows the wave speed for one lap around the detonation channel with run conditions of $\dot{m}_{total}$ = 164 lbs/min and ϕ = 1.15. Red arrows mark wave passage past an instrumentation port. The black arrow marks wave passage past the predetonation port. The method to determine wave speed as the detonation wave travels around the detonation channel was discussed in section 3.8.

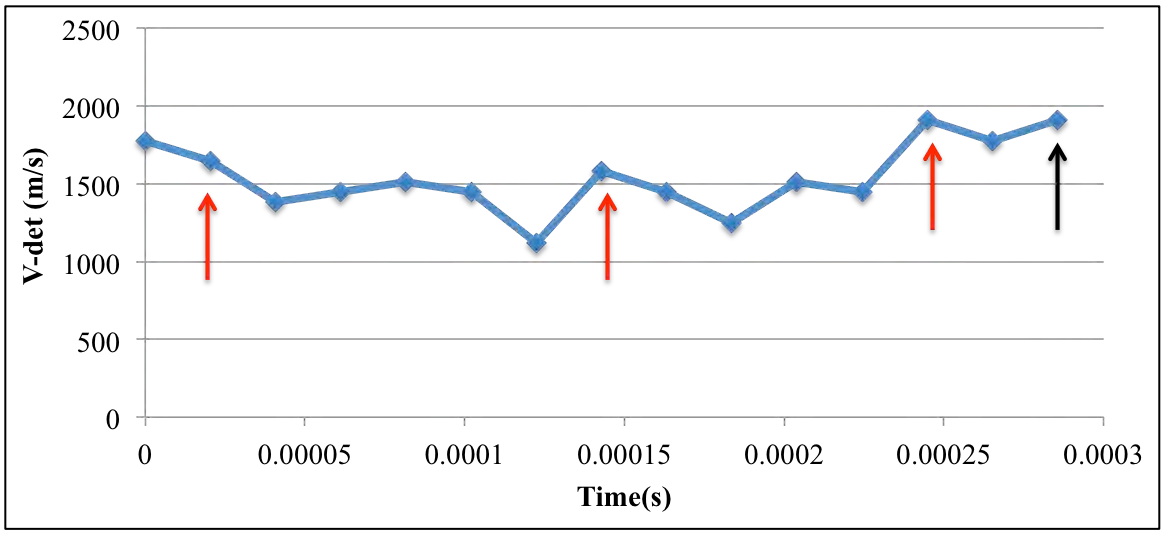

Figure 42. Velocity track for one lap around detonation channel with no reversal

Figure 42 shows that wave speed decreases after the detonation front passes a port. Similar analysis was performed for four other wave revolutions under different run conditions (see Appendix F for data and plots). Analysis showed for waves traveling greater than 1000 m/s, their velocity decreased after passing a port 84% of the time.

It is hypothesized that the decrease in velocity is caused by shock wave reflection off the ports in the detonation channel (instrumentation and blank ports). As the detonation travels past the port, a shock wave is reflected in the opposite direction of wave travel. The reflected shock wave strips energy strips energy from the detonation. The reduced energy ultimately results in a decrease in velocity. This hypothesis could also explain why two waves sometimes form traveling in opposite directions, since it has been proven that shock waves can start detonations.

CHAPTER 5. CONCLUSIONS AND RECOMMENDATIONS

5.1 Conclusions

The goal of this research was to develop and install a new RDE, determine its operational mass flow rates and equivalence ratios for standard air, and characterize the detonation wave as it travels around the detonation channel. The new 6 in RDE allows for easy adjustment of five critical variables and provides a flexible platform upon which RDE research can be performed. A lower and left hand boundary was found for successful operation. The lower boundary is defined by a linear relationship between equivalence ratio and fuel mass flow rate. The left hand boundary is defined by a minimum equivalence ratio of approximately 0.94. Detonation velocities were higher than those previously recorded and depended on total mass flow rates.

It can be asserted that mixing between the oxidizer and fuel in the new RDE is better than mixing in previous rigs. This is reflected in successful operation at lower equivalence ratios and higher detonation velocities than those previously achieved. Without the proprietary knowledge of previous injection schemes, one cannot definitively state as to why the new scheme is better.

The average detonation velocities in the 6 in RDE were less than V_{CJ}. High-speed video analysis gave two insights. The first insight was that V_{CJ} is achievable in an RDE. V_{CJ} was observed many times throughout the high-speed analysis. The second insight is that irregularities in the detonation channel remove energy from the detonation wave by reflecting shocks in the opposite direction. The reflected shocks also contribute to

unsteadiness during operation by sometimes starting detonations in the opposite direction.

5.2 Recommendations

This work has developed a flexible platform upon which RDE research can be performed. This work has also analyzed the detonation wave from a top down view. Future work should focus on obtaining a side view of the detonation wave in order to visualize the detonation front from another perspective. This may ultimately lead to one-way ignition and rotation of the detonation wave at V_{CJ}.

Mapping the RDE operational space on ethylene and air would be a next logical step on the path to running jet fuel and air. The fuel plate should be replaced with one designed for ethylene.

To better examine sizing effects (6 in RDE versus 3 in RDE) a 3 in RDE with the same design and injection scheme should be installed.

Finally, studies into achieving consistent, unidirectional detonation and predetonation in the RDE should be done as a precursor to integration of downstream components.

APPENDIX A. CAD DRAWINGS OF RDE

Bottom Plate

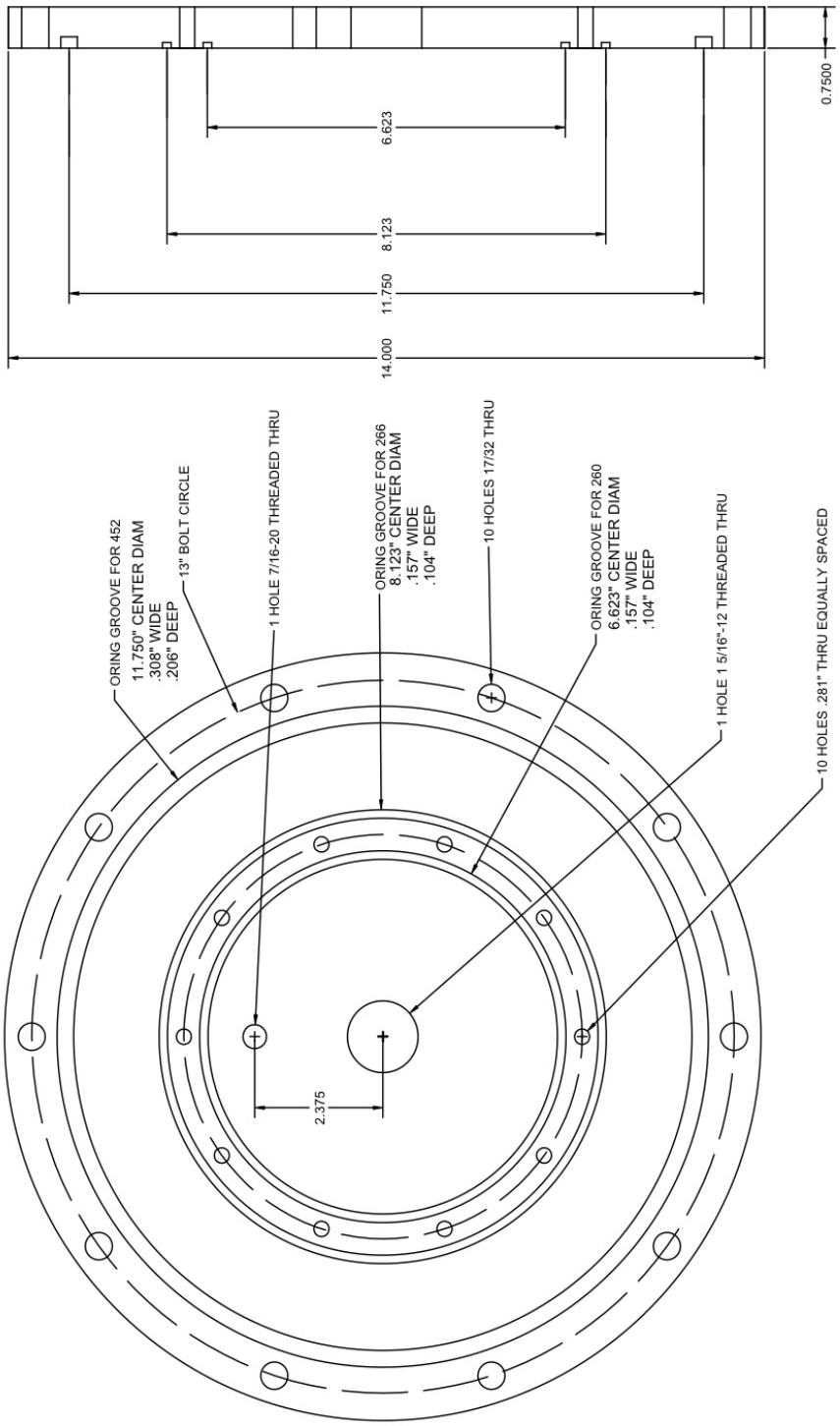

Oxidizer Main Ring

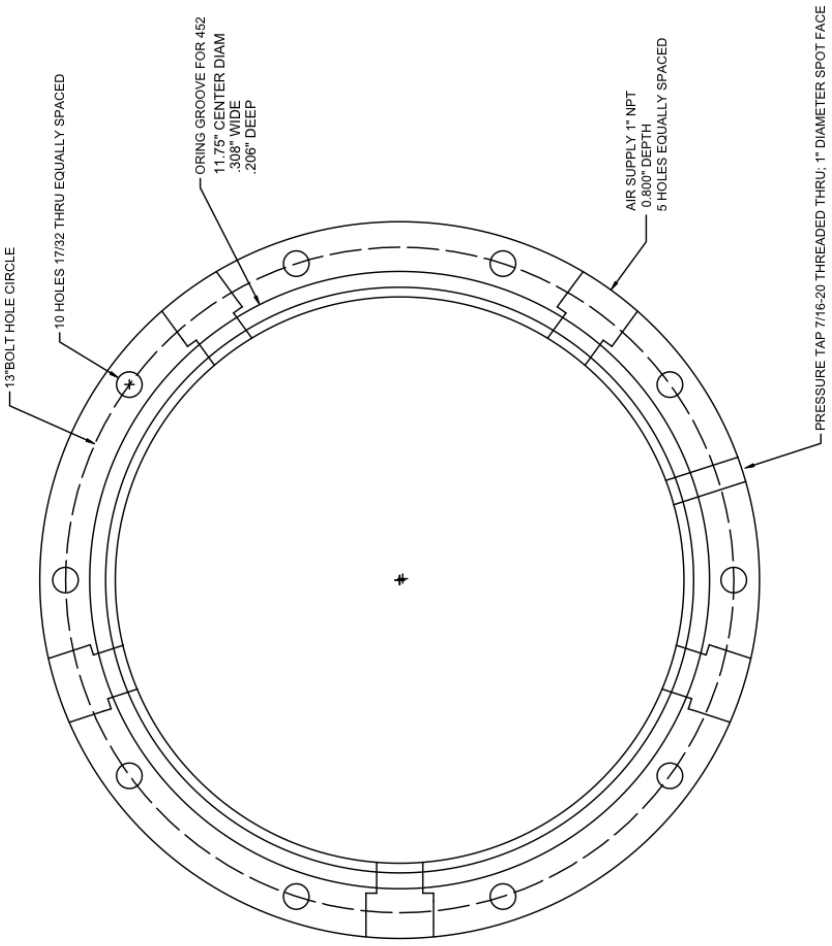

Oxidizer Spacer

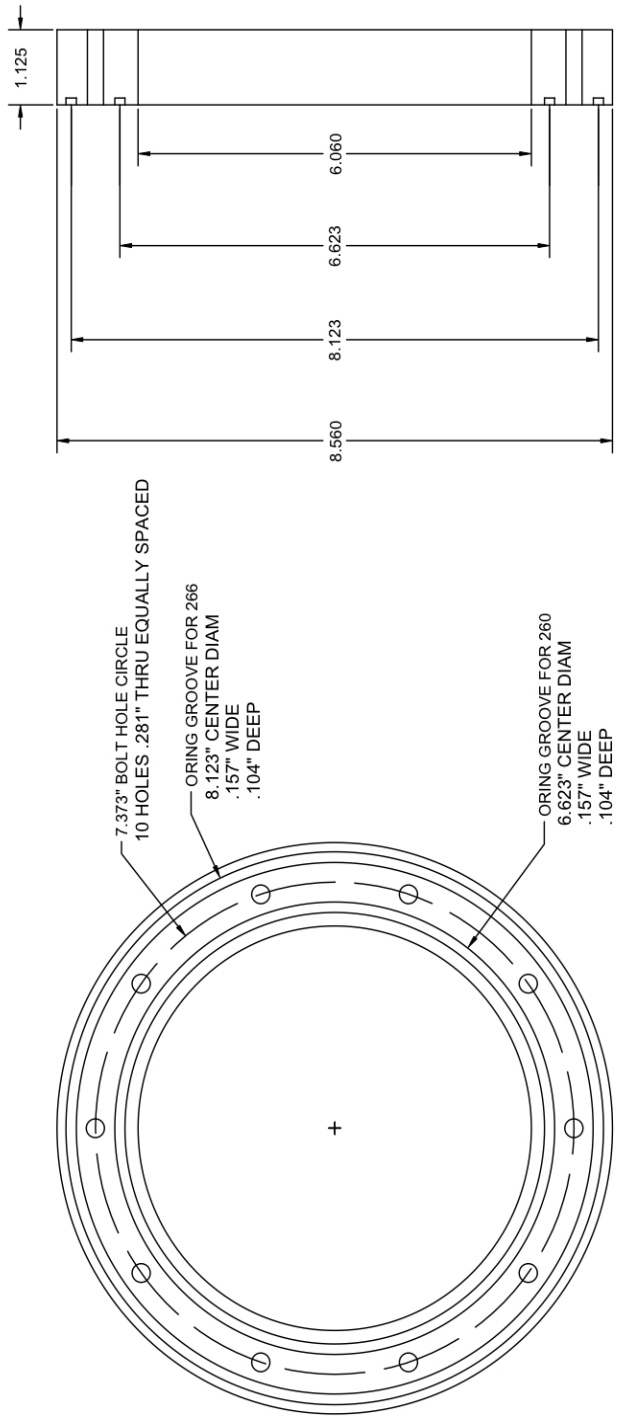

Fuel plate

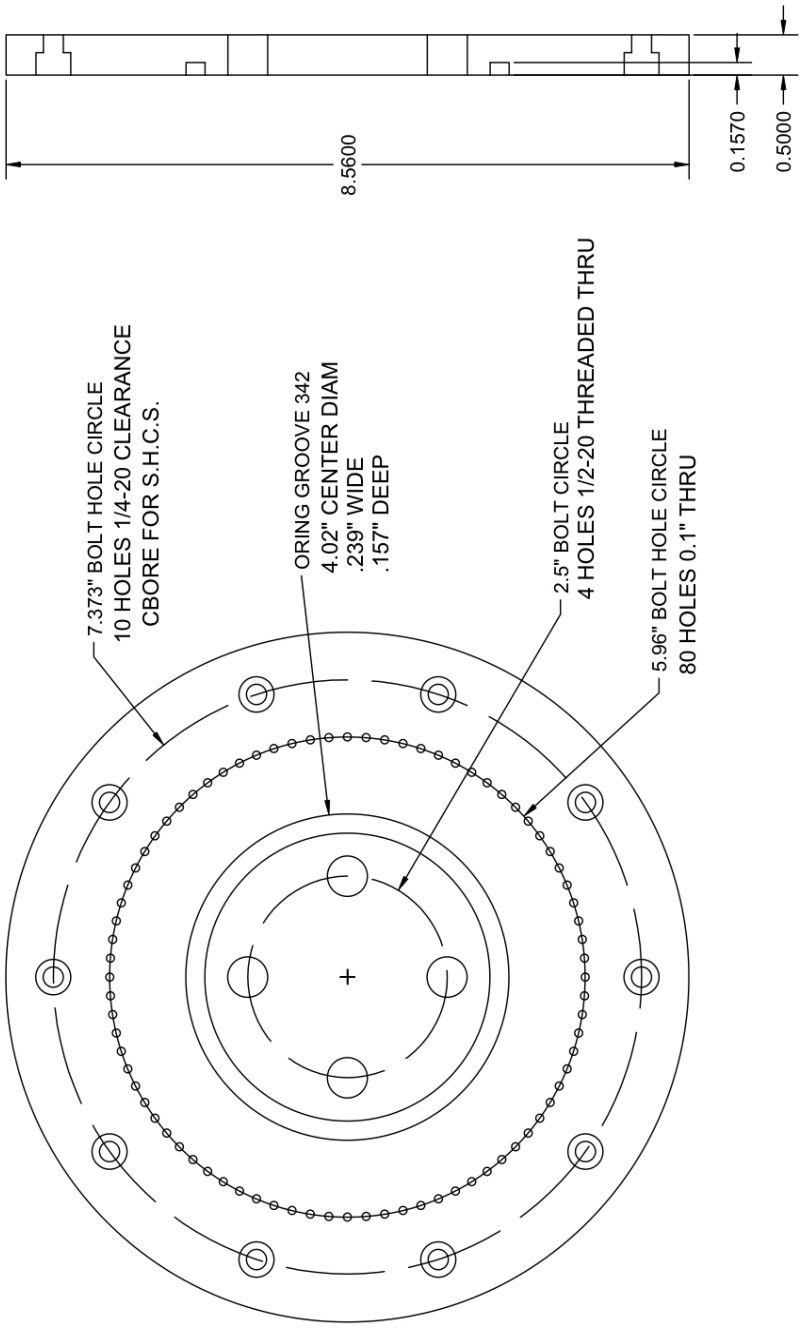
8.5600
0.1570
0.5000
7.373" BOLT HOLE CIRCLE
10 HOLES 1/4-20 CLEARANCE
CBORE FOR S.H.C.S.
ORING GROOVE 342
4.02" CENTER DIAM
.239" WIDE
.157" DEEP
2.5" BOLT CIRCLE
4 HOLES 1/2-20 THREADED THRU
5.96" BOLT HOLE CIRCLE
80 HOLES 0.1" THRU

Top Ring

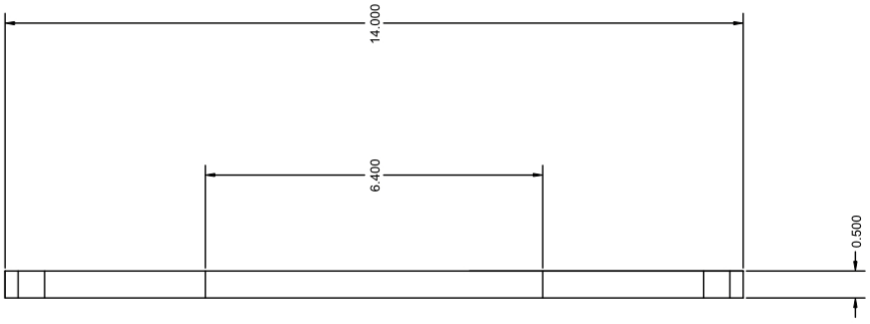

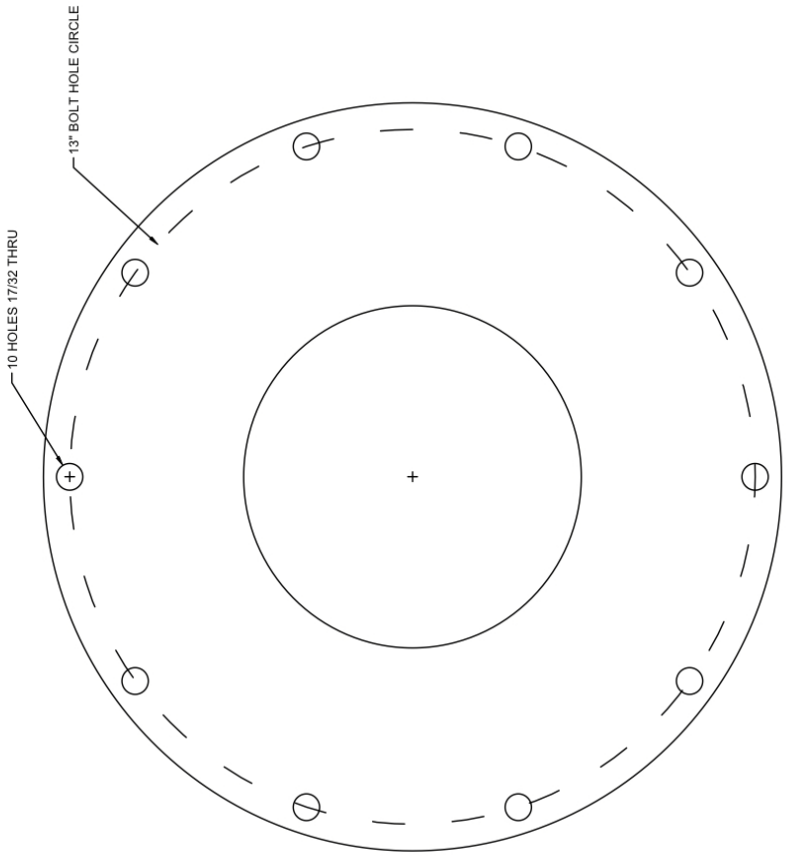

Outer Body

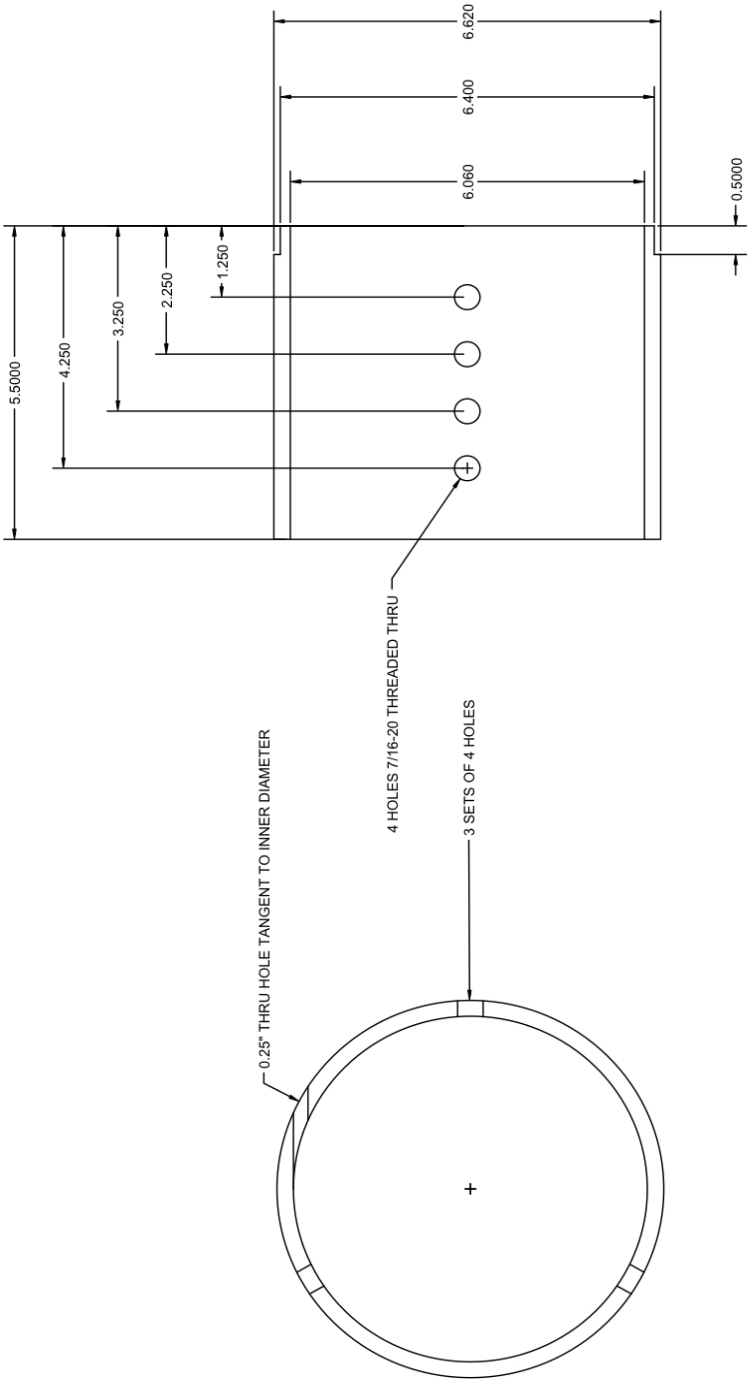
6.620
6.400
6.060
0.5000
1.250
2.250
3.250
4.250
5.5000
4 HOLES 7/16-20 THREADED THRU
3 SETS OF 4 HOLES
0.25" THRU HOLE TANGENT TO INNER DIAMETER

Center Body

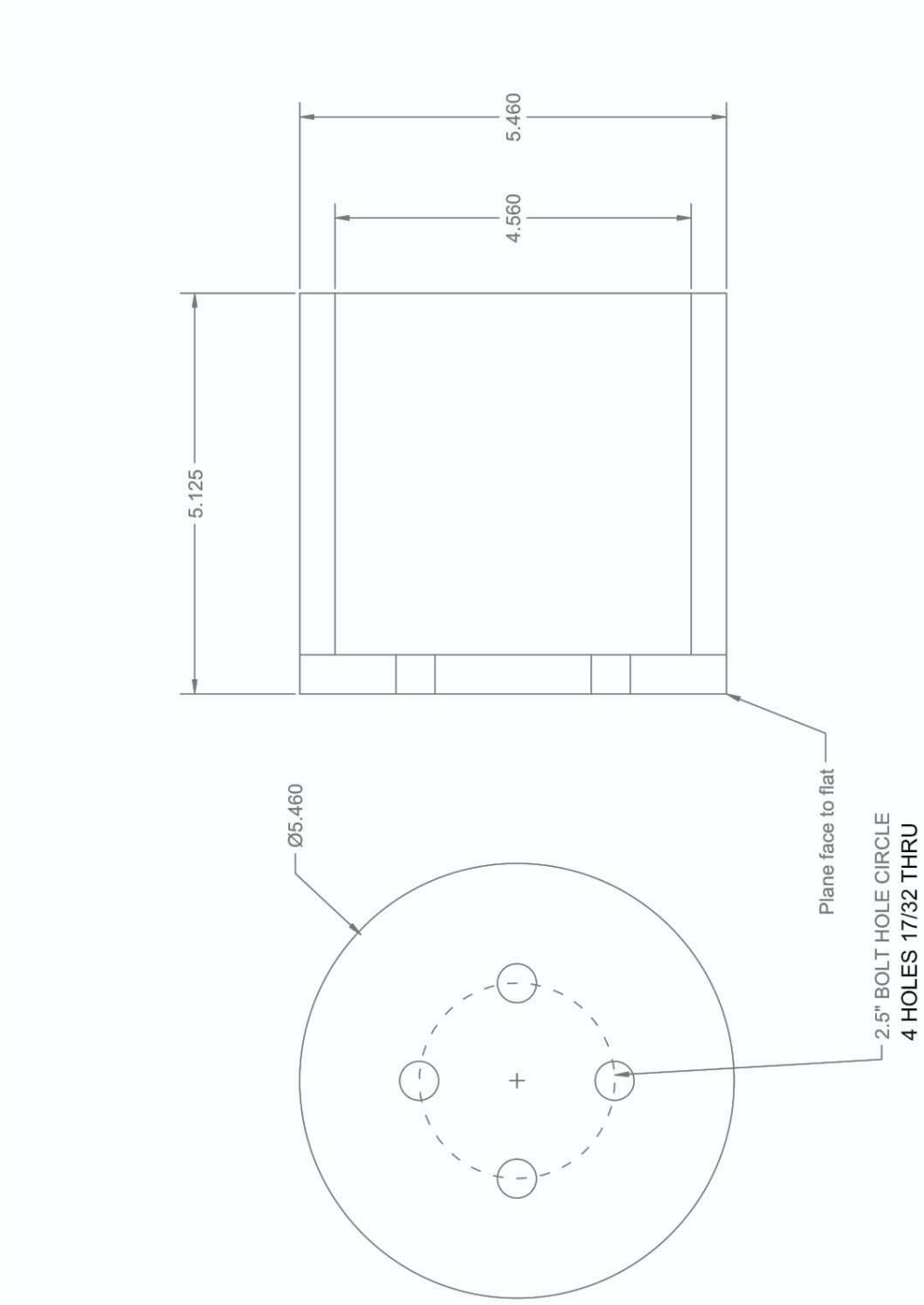
5.460
4.560
5.125
Plane face to flat
Ø5.460
2.5" BOLT HOLE CIRCLE
4 HOLES 17/32 THRU

APPENDIX B. DATA REDUCTION CODE

The following code was written and validated by Russo[11]. The code remains the same as in her work except for the number of points required to constitute a pressure peak and the hold time to find a pressure peak. Other than these two small adjustments, as outlined in Chapter 3, the code remains entirely the same as outlined and developed in Russo's work[11].

```
function
[wsTime,waveSpeed,blah,err_bias_diam,err_bias_t1,err_bias_t2,err_bias,avg_detSpeed,p
ercent_err] = test(data,chan,dist)
% [time,speed] = test(data,chan,dist)
%
%   Test calculates time of flight wave speed for a single PCB pressure ducer in
%   a RDE channel and returns a vector of waves speeds and their associated run
%   times. Wave detection is based on the ion probe drop algoritm used in
%   PTFinder.
%
%   Input: data - row array of pressure data. First row must be time.
%          chan - channel to calculate wave speed from
%          dist - circufrence of channel
%
%   Output: time - vector of times of each speed measurement
%           speed - vector of wave speeds
close all

% Extract time and signal from the array
time = data(1,:);
trace = data(chan+1,:);


% Calculate a moving average, and a threshold
avg = smooth(trace,1001,'moving');
stdev = std(detrend(trace,'linear',(1000:3000:999999)'));
thresh = (avg+stdev)';

% Setup looping variables
ind = find(trace > thresh);  % indices of data points above threshold
ctr = 0;                     % point counter
passes =[0 0 0 0];           % indices of wave passes
iPass = 1;                   % current wave pass number
latch = false;               % logical variable for preventing false triggers

% loop through data points above threshold
for i = 1:length(ind)-1
   % ignore data within 240us of a wave pass
   if latch
```

```
        if (time(ind(i))-time(passes(iPass-1))) > 240e-6
        else
            continue
        end
    end

    % check for a set of two points in a row
    if ind(i) == ind(i+1)-1
        % increment the counter if points are adjacent
        ctr = ctr+1;
    else
        % reset the counter if not
        ctr = 0;
    end %if

    % Record the time and begin ignoring data when a wave pass is detected
    if ctr >= 2
        passes(iPass) = ind(i-1);  % time of wave pass
        iPass = iPass+1;           % keep track of the current wave pass
        latch = true;              % set a logical to ignore data for the next 60us
        ctr = 0;                   % reset the counter for the next pass
    end %if

end %for i

% Calculate times and wave speeds
wsTime = (time(passes(1:end-1))'+time(passes(2:end))')/2; % average of two passes
waveSpeed = dist./diff(time(passes)');          % change in time over circumfrence
figure
plot(wsTime,waveSpeed,'.')
xlabel('Time (s)')
ylabel('Speed (m/s)')
title('Wave Speed')
avgspeed=mean(waveSpeed)
stdev_vel=std(waveSpeed);

blah=1;
for iii=1:length(waveSpeed)
    if waveSpeed(iii)<1000
        combustSpeed(blah)=waveSpeed(iii);
        blah=blah+1;
    end
end
avg_combustSpeed=mean(combustSpeed)

blah=1;
```

```
for iii=1:length(waveSpeed)
   if (waveSpeed(iii)>1000 & waveSpeed(iii)<1960);
      detSpeed(blah)=waveSpeed(iii);
      blah=blah+1;
   end
end
avg_detSpeed=mean(detSpeed)
mode_detSpeed=mode(detSpeed);
speed_ratio=avg_combustSpeed/avg_detSpeed;

waveSpeed_avg=smooth(waveSpeed,51,'moving');
figure
plot(wsTime,waveSpeed_avg,'.')
xlabel('Time (s)')
ylabel('Average Speed (m/s)')
title('Wave Speed, Moving Average')

figure
hist(waveSpeed,150)
xlabel('Velocity (m/s)')

blah=diff(time(passes)'); %delta t (sec)
err_bias_diam=(3.141592654*.000127)./blah'; %know diam to .005 in
err_bias_t1=(dist*(.5*10^-6))./((time(passes(1:end-1))).^2); %know time to .5 micro sec
err_bias_t2=(-dist*(.5*10^-6))./((time(passes(2:end))).^2); %know time to .5 micro sec
err_bias=(err_bias_diam.^2+err_bias_t1.^2+err_bias_t2.^2).^.5;
err_bias_use=mean(err_bias);

err_precision=2*stdev_vel %for 95% confidence interval, from pg 185 of Intro to
Engineering Experimentation

err_tot=(err_bias_use^2+err_precision^2)^.5;

percent_err=(err_tot/avgspeed)*100;
```

APPENDIX C. OP SPACE DATA BASED ON TOTAL FLOW RATE

Table 1. Equivalence Ratio and Total Mass Flow Rate for All Runs

Unsuccessful		Successful	
Φ	**m-dot total (lbs/min)**	**Φ**	**m-dot total (lbs/min)**
0.93	93.3	1.23	151.2
1.05	93.6	1.27	150.3
1.23	94.1	1.12	149.6
1.37	94	1.45	155.0
1.54	94.5	1.29	157.0
1.07	69.1	1.13	165.4
1.29	69.7	1.07	167.3
1.4	69.9	0.95	158.7
1.12	52.1	1.05	159.2
1.26	52.5	1.05	159.2
1.43	52.6	1.09	159.4
1.16	43.4	1.19	159.8
1.31	43.6	1.24	160.0
0.97	102.1	1.31	160.3
1.02	103.9	1.37	160.6
1.21	103.9	1.01	172.2
1.2	105.6	1.08	172.5
1.11	104.2	1.11	171.2
1.2	105.0	0.99	197.5
1.06	149.3	0.94	197.2
0.65	167.5	1.12	198.2
0.86	163.0	0.92	179.7
0.88	158.4	0.92	179.7
0.9	158.5	1.11	180.6
0.88	172.2	1.22	181.0
0.93	171.8	1.22	181.0
0.77	198.1	0.97	220.3
0.87	196.8	1.15	164.0
0.88	179.3	0.95	163.1
0.88	179.4	1.17	167.6
0.89	128.7	1.03	216.2
0.97	128.9	0.98	215.9
1.03	129.2	0.94	213.9
1.1	129.4	1.03	161.2
1.2	129.8	0.97	166
0.88	162.8		
0.93	163.0		
0.87	215.2		
0.91	213.7		
0.86	233.5		
0.89	233.8		
0.92	233.9		
0.94	233.9		
0.94	166.0		

APPENDIX D. OP SPACE DATA BASED ON FUEL FLOW RATE

Table 2. Equivalence Ratios and Fuel Flow Rate for Successful Runs

Successful	
Φ	**m-dot fuel (lbs/min)**
1.15	5.33
0.95	4.45
1.17	5.56
1.03	6.36
0.98	6.01
0.94	5.74
0.95	4.31
1.05	4.75
1.05	4.75
1.09	4.95
1.19	5.38
1.24	5.64
1.31	5.92
1.37	6.19
1.01	4.97
1.08	5.29
1.11	5.43
0.99	5.58
0.94	5.29
1.12	6.32
0.95	4.75
0.95	4.75
1.11	5.7
1.22	6.24
1.22	6.24
0.97	6.1
0.95	4.25
0.95	4.25
1.09	4.95
1.31	5.92
1.37	6.19
1.24	5.64
1.19	5.38
1.05	4.75
0.95	4.45
0.94	5.74
0.95	4.31
0.94	5.29
0.95	4.75
0.95	4.25

Bottom Boundary	
0.95	4.25
1.31	5.92
1.37	6.19
1.24	5.64
1.19	5.38
1.05	4.75

Left Boundary	
0.95	4.45
0.94	5.74
0.95	4.31
0.94	5.29
0.95	4.75
0.95	4.25

APPENDIX E. AVERAGE MASS FLOW AND V-DET DATA

Table 3. Total Mass Flows and Detonation Velocities with Wave Speed Error

m-dot total (lbs/min)	Average m-dot total (lbs/min)	Φ	V-det (m/s)	Average V-det (m/s)	Error (%)
159.8	160.2	1.19	1390	1409	35.8
160.0		1.24	1398		39.3
160.3		1.31	1400		43.6
160.6		1.37	1448		40.7
172.2	172.0	1.01	1443	1440	35.0
172.5		1.08	1436		35.9
171.2		1.11	1441		36.7
197.5	180.3	0.99	1524	1481	45.0
197.2		0.94	1508		35.6
198.2		1.12	1513		33.1
179.7	197.6	0.92	1470	1515	38.4
179.7		0.92	1444		33.2
181.0		1.22	1522		34.3
181.0		1.22	1487		37.6
220.3	220.3	0.97	1563	1563	39.1

APPENDIX F. HIGH-SPEED VIDEO ANALYSIS

Table 4. Raw High-Speed Data for m-dot = 164 lbs/min, Φ = 1.15

Lap 1	Polar Position	Degrees Traveled	Distance Traveled (m)	Time (s)	V-det (m/s)
frame interval = 20.4μs	110				
m-dot = 164 lbs/min	89	21	0.028	0	1383
Φ = 1.15	60	29	0.039	0.0000204	1910
	38	22	0.030	0.0000408	1449
	15	23	0.031	0.0000612	1514
	348	27	0.036	0.0000816	1778
	327	21	0.028	0.000102	1383
	303	24	0.032	0.0001224	1580
	279	24	0.032	0.0001428	1580
	260	19	0.026	0.0001632	1251
	238	22	0.030	0.0001836	1449
	211	27	0.036	0.000204	1778
	185	26	0.035	0.0002244	1712
	162	23	0.031	0.0002448	1514
	135	27	0.036	0.0002652	1778
	112	23	0.031	0.0002856	1514

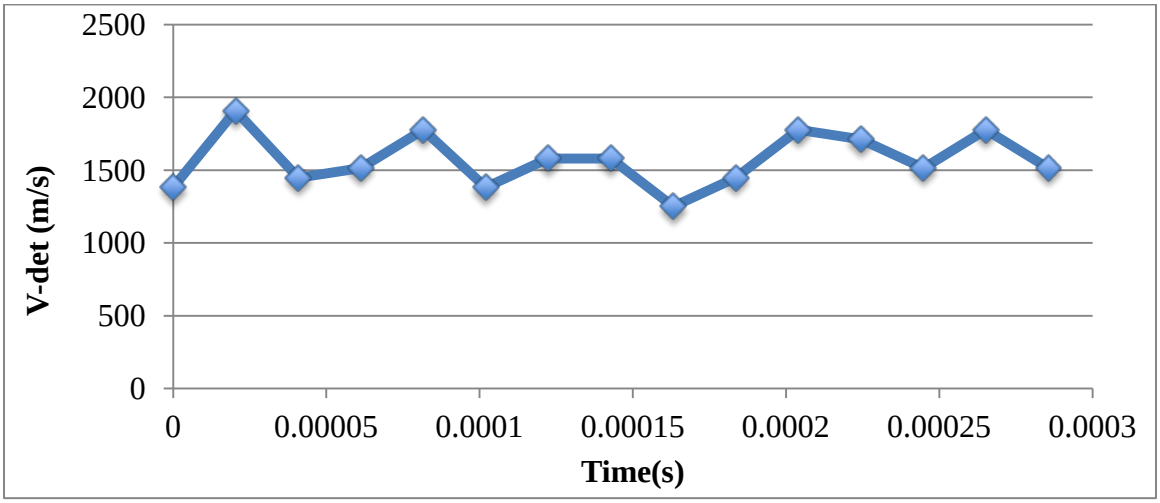

Figure 43. Velocity Track for m-dot = 164 lbs/min, Φ = 1.15

Table 5. Raw High-Speed Data for m-dot = 163.1 lbs/min, Φ = 0.95

Lap 2	Polar Position	Degrees Traveled	Distance Traveled (m)	Time (s)	V-det (m/s)
frame interval = 20.4μs	253				
m-dot = 163.1 lbs/min	226	27	0.036	0	1778
Φ = 0.95	201	25	0.034	0.0000204	1646
	180	21	0.028	0.0000408	1383
	158	22	0.030	0.0000612	1449
	135	23	0.031	0.0000816	1514
	113	22	0.030	0.000102	1449
	96	17	0.023	0.0001224	1119
	72	24	0.032	0.0001428	1580
	50	22	0.030	0.0001632	1449
	31	19	0.026	0.0001836	1251
	8	23	0.031	0.000204	1514
	346	22	0.030	0.0002244	1449
	317	29	0.039	0.0002448	1910
	290	27	0.036	0.0002652	1778
	261	29	0.039	0.0002856	1910

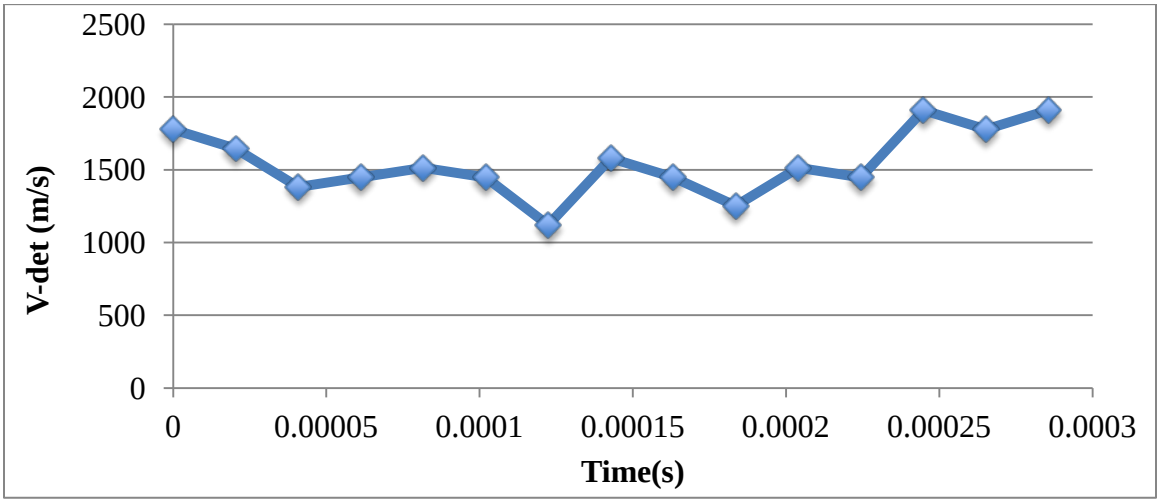

Figure 44. Velocity Track for m-dot = 163.1 lbs/min, Φ = 0.95

Table 6. Raw High-Speed Data for m-dot = 164.1 lbs/min, Φ = 1.15

Lap 3	Polar Position	Degrees Traveled	Distance Traveled (m)	Time (s)	V-det (m/s)
frame interval = 20.4μs	210				
m-dot = 164.1 lbs/min	183	27	0.036	0	1778
Φ = 1.15	160	23	0.031	0.0000204	1514
	136	24	0.032	0.0000408	1580
	112	24	0.032	0.0000612	1580
	90	22	0.030	0.0000816	1449
	69	21	0.028	0.000102	1383
	41	28	0.038	0.0001224	1844
	17	24	0.032	0.0001428	1580
	352	25	0.034	0.0001632	1646
	322	30	0.040	0.0001836	1975
	297	25	0.034	0.000204	1646
	270	27	0.036	0.0002244	1778
	240	30	0.040	0.0002448	1975
	212	28	0.038	0.0002652	1844
	182	30	0.040	0.0002856	1975

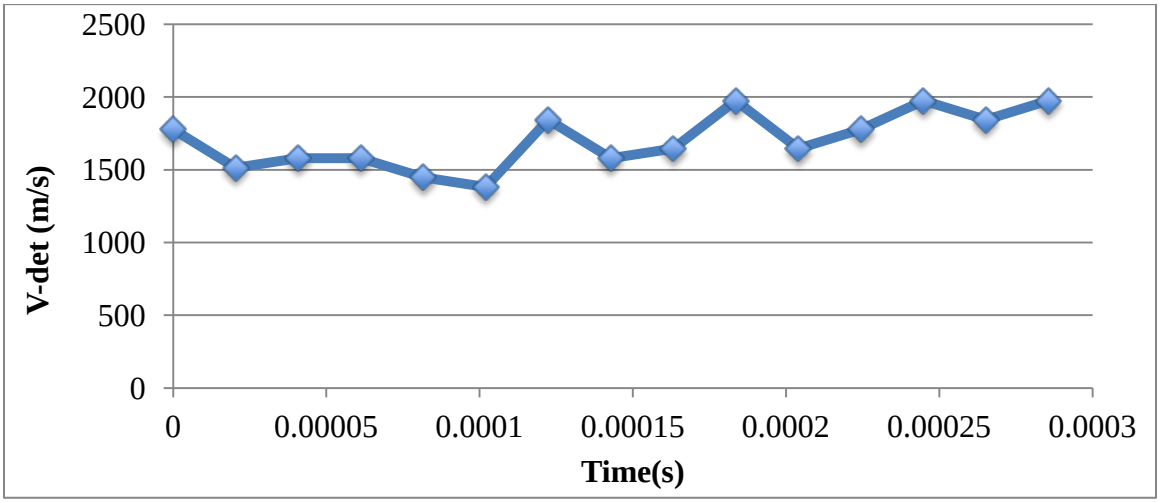

Figure 45. Velocity Track for m-dot = 164.1 lbs/min, Φ = 1.15

Table 7. Raw High-Speed Data for m-dot = 215.9 lbs/min, Φ = 0.98

Lap 4	Polar Position	Degrees Traveled	Distance Traveled (m)	Time (s)	V-det (m/s)
frame interval = 20.4μs	190				
m-dot = 215.9 lbs/min	165	25	0.034	0	1646
Φ = 0.98	138	27	0.036	0.0000204	1778
	115	23	0.031	0.0000408	1514
	91	24	0.032	0.0000612	1580
	72	19	0.026	0.0000816	1251
	46	26	0.035	0.000102	1712
	26	20	0.027	0.0001224	1317
	3	23	0.031	0.0001428	1514
	341	22	0.030	0.0001632	1449
	312	29	0.039	0.0001836	1910
	287	25	0.034	0.000204	1646
	272	15	0.020	0.0002244	988
	248	24	0.032	0.0002448	1580
	226	22	0.030	0.0002652	1449
	201	25	0.034	0.0002856	1646

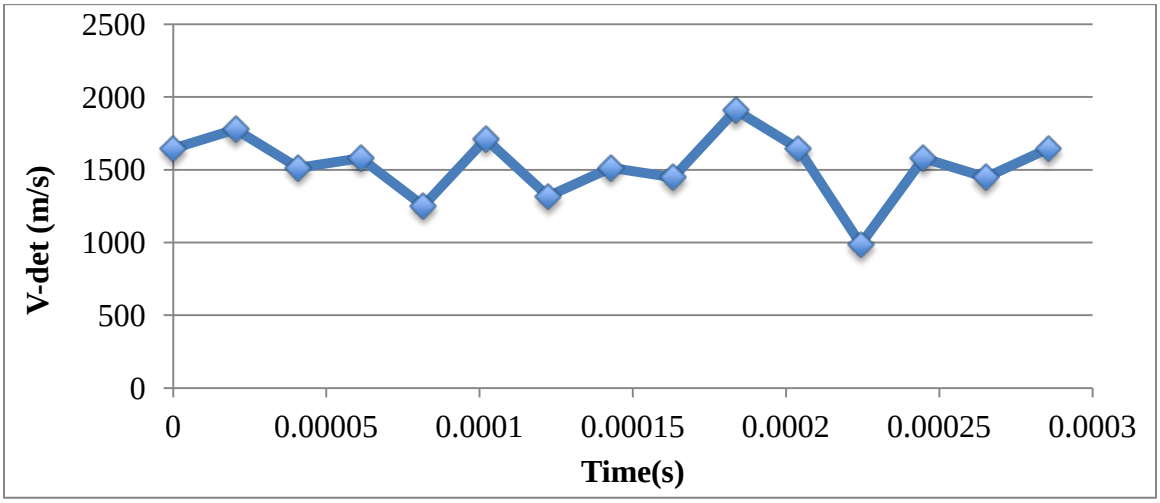

Figure 46. Velocity Track for m-dot = 215.9 lbs/min, Φ = 0.98

Table 8. Raw High-Speed Data for m-dot = 160 lbs/min, Φ = 1.24

Lap 5	Polar Position	Degrees Traveled	Distance Traveled (m)	Time (s)	V-det (m/s)
frame interval = 20.4μs	280				
m-dot = 160 lbs/min	236	44	0.059	0	1832
Φ = 1.24	197	39	0.052	3.22581E-05	1624
	152	45	0.060	6.45161E-05	1874
	112	40	0.054	9.67742E-05	1666
	68	44	0.059	0.000129032	1832
	30	38	0.051	0.00016129	1582
	8	22	0.030	0.000193548	916
	323	45	0.060	0.000225806	1874
	280	43	0.058	0.000258065	1791
	242	38	0.051	0.000290323	1582

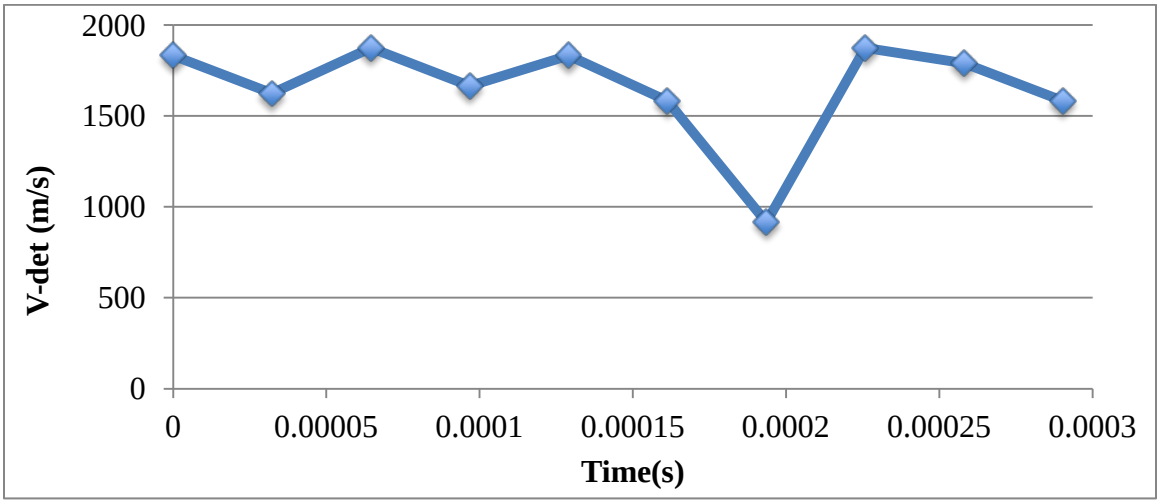

Figure 47. Velocity Track for m-dot = 160 lbs/min, Φ = 1.24

Table 9. Raw High-Speed Data for Predetonation

Predet	Polar Position	Degrees Traveled	Distance Traveled (m)	Time (s)	V-det (m/s)
frame interval = 20.4µs	270				
Wave 1	260	10	0.013	0	658
	250	10	0.013	0.0000204	658
	235	15	0.020	0.0000408	988
	220	15	0.020	0.0000612	988
	205	15	0.020	0.0000816	988
	185	20	0.027	0.000102	1317
	159	26	0.035	0.0001224	1712
	136	23	0.031	0.0001428	1514
	115	21	0.028	0.0001632	1383
	93	22	0.030	0.0001836	1449
Wave 2	270				
	280	10	0.013	0	658
	292	12	0.016	0.0000204	790
	307	15	0.020	0.0000408	988
	323	16	0.021	0.0000612	1054
	345	22	0.030	0.0000816	1449
	4	19	0.026	0.000102	1251
	23	19	0.026	0.0001224	1251
	47	24	0.032	0.0001428	1580
	70	23	0.031	0.0001632	1514
	90	20	0.027	0.0001836	1317

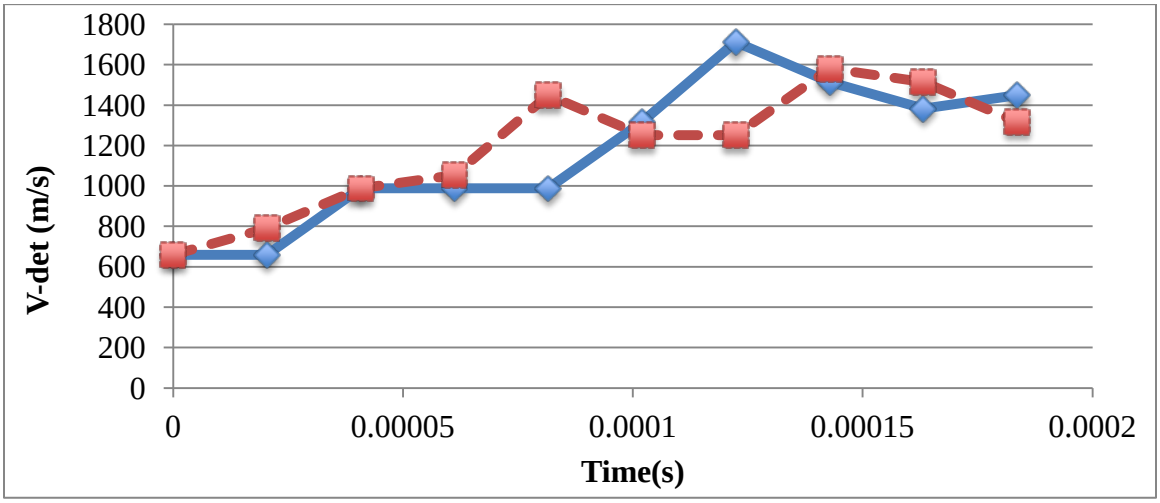

Figure 48. Velocity Track for Predetonation

REFERENCES

1. Bussing, T. and G. Pappas. "An Introduction to Pulse Detonation Engines," *32nd Aerospace Sciences Meeting and Exhibit*. Reno, NV, January 1994. AIAA 94-0263.

2. Voitsekhovskii, B. V., V. V. Mitrofanov, and M. E. Topchian. "Investigation of the Structure of Detonation Waves in Gases," *Symposium (International) on Combustion*, 12: 829-837 (1969).

3. Bykovskii, Fedor A., Sergey A. Zhdan, and Evgenii F. Vedernikov. "Continuous Spin Detonations," *Journal of Propulsion and Power*, 22: 1204-1216 (2006).

4. Schwer, Douglas A. and K. Kailasanath. "Numerical Investigation of Rotating Detonation Engines," *46th Joint Propulsion Conference and Exhibit.* Nashville, TN, 2010. AIAA 2010-6880.

5. Chapman, D.L., "On the Rate of Explosion of Gases," Philosophical Magazine, 47: 90-103 (1899).

6. Zeldovich, Y.B., "The Theory of the Propogation of Detonation in Gaseous Systems," Experimental and Theoretical Physics, S.S.S.R., 10: 542 (1940).

7. Hishida, Manabu, Toshi Fujiwara, and Piotr Wolanski. "Fundamentals of Rotating Detonations," *Shock Waves*, 19 (2009).

8. Schwer, Douglas A. and K. Kailasanath. "Feedback into Mixture Plenums in Rotating Detonation Engines," *50th Aerospace Sciences Meeting.* Nashville, TN, 2012. AIAA 2012-0617.

9. Davidenko, Dmitry M, Iskender Gokalp, and Alexey N. Kudryavstev. "Numerical Study of the Continuous Detonation Wave Rocket Engine," *15th International Space Planes and Hypersonic Systems and Technologies Conference*. Dayton, OH. AIAA 2008-2680

10. Thomas, Levi M., et al. "Buildup and Operation of a Rotating Detonation Engine," *49th AIAA Aerospace Sciences Meeting*. Orlando, 2011. AIAA 2011-602.

11. Russo, Rachel M, Paul King, Fred Schauer, and Levi Thomas. "Characterization of Pressure Rise Across a Continuous Detonation Engine," Joint Propulsion Conference. June 2011. AIAA-2011-6046.

12. Suchocki, Jim. "Operational Space and Characterization of a Rotating Detonation Engine Using Hydrogen and Air," The Ohio State University, January 2012. Thesis.

13. Oates, Gordon C. *Aerothermodynamics of Gas Turbine and Rocket Propulsion*. Reston, VA: AIAA, 1997.

REPORT DOCUMENTATION PAGE

Form Approved
OMB No. 074-0188

1. REPORT DATE *(DD-MM-YYYY)*	**2. REPORT TYPE**	**3. DATES COVERED** *(From – To)*
22-03-2012	Master's Thesis	Oct 2010 – March 2012

TITLE AND SUBTITLE

Development and Testing of a Rotating Detonation Engine Run on Hydrogen and Air

5a. CONTRACT NUMBER

5b. GRANT NUMBER

5c. PROGRAM ELEMENT NUMBER

6. AUTHOR(S)

Shank, Jason C. 2Lt, USAF

5d. PROJECT NUMBER

5e. TASK NUMBER

5f. WORK UNIT NUMBER

7. PERFORMING ORGANIZATION NAMES(S) AND ADDRESS(S)
Air Force Institute of Technology
Graduate School of Engineering and Management (AFIT/ENY)
2950 Hobson Way, Building 640
WPAFB OH 45433-8865

8. PERFORMING ORGANIZATION REPORT NUMBER

AFIT/GAE/ENY/12-M36

9. SPONSORING/MONITORING AGENCY NAME(S) AND ADDRESS(ES)

Intentionally left blank

10. SPONSOR/MONITOR'S ACRONYM(S)

11. SPONSOR/MONITOR'S REPORT NUMBER(S)

12. DISTRIBUTION/AVAILABILITY STATEMENT
APPROVED FOR PUBLIC RELEASE; DISTRIBUTION UNLIMITED.

13. SUPPLEMENTARY NOTES

14. ABSTRACT

Rotating detonation engines (RDEs) have the potential for greater efficiencies over conventional engines by utilizing pressure gain combustion. A new modular RDE (6 in diameter) was developed and successfully run on hydrogen and standard air. The RDE allows for variation of injection scheme and detonation channel widths. Tests provided the operational space of the new RDE as well as characterized detonation unsteadiness. It was found that a smaller equivalence ratio than previous was required to obtain continuous detonations. Also discovered was V_{CJ} was reached in the RDE, but not sustained.

15. SUBJECT TERMS
Rotating detonation engine, detonation, pressure gain combustion

16. SECURITY CLASSIFICATION OF:			**17. LIMITATION OF ABSTRACT**	**18. NUMBER OF PAGES**	**19a. NAME OF RESPONSIBLE PERSON**
a. REPORT	**b. ABSTRACT**	**c. THIS PAGE**			Dr. Paul King
U	**U**	**U**	**UU**	84	**19b. TELEPHONE NUMBER** *(Include area code)* (937) 255-6565, ext 4628 (Paul.King@afit.edu)

Standard Form 298 (Rev. 8-98)
Prescribed by ANSI Std. Z39-18